AGU ADVANCING EARTH AND SPACE SCIENCES

JGR Atmospheres

RESEARCH ARTICLE
10.1029/2023JD039091

Global Observations of Tropospheric Bromine Monoxide (BrO) Columns From TROPOMI

Yuyang Chen[1], Song Liu[1], Lei Zhu[1,2], Sora Seo[3,4], Andreas Richter[3], Xicheng Li[1], Ao Ding[1], Wenfu Sun[5], Lei Shu[1,6], Xuan Wang[7,8], Pieter Valks[4], Francois Hendrick[5], Theodore K. Koenig[9,10], Rainer Volkamer[9], Bin Bai[11], Dakang Wang[1,12], Dongchuan Pu[1], Shuai Sun[1], Juan Li[1], Xiaoxing Zuo[1], Weitao Fu[1], Yali Li[1], Peng Zhang[1], Xin Yang[1,2], and Tzung-May Fu[1,2]

[1]School of Environmental Science and Engineering, Southern University of Science and Technology, Shenzhen, China, [2]Guangdong Provincial Observation and Research Station for Coastal Atmosphere and Climate of the Greater Bay Area, Shenzhen, China, [3]Institute of Environmental Physics, University of Bremen, Bremen, Germany, [4]Deutsches Zentrum für Luft- und Raumfahrt (DLR), Institut für Methodik der Fernerkundung (IMF), Oberpfaffenhofen, Germany, [5]Belgian Institute for Space Aeronomy (BIRA-IASB), Brussels, Belgium, [6]School of Geographical Sciences, Fujian Normal University, Fuzhou, China, [7]School of Energy and Environment, City University of Hong Kong, Hong Kong SAR, China, [8]Low-Carbon and Climate Impact Research Centre, City University of Hong Kong, Hong Kong SAR, China, [9]Department of Chemistry and CIRES, University of Colorado at Boulder, Boulder, CO, USA, [10]Now at State Key Joint Laboratory of Environmental Simulation and Pollution Control, BIC-ESAT and IJRC, College of Environmental Sciences and Engineering, Peking University, Beijing, China, [11]School of Earth and Atmospheric Sciences, Georgia Institute of Technology, Atlanta, GA, USA, [12]School of Geography and Remote Sensing, Guangzhou University, Guangzhou, China

Key Points:

- We present the retrieval and evaluation of tropospheric BrO columns from TROPOspheric Monitoring Instrument (TROPOMI)
- Our high-resolution BrO product identifies small-scale emission sources on a daily scale
- A blowing snow aerosol bromine scheme with reduced snow salinity improves agreement between the model and TROPOMI

Supporting Information:

Supporting Information may be found in the online version of this article.

Correspondence to:

S. Liu and L. Zhu,
lius7@sustech.edu.cn;
zhul3@sustech.edu.cn

Citation:

Chen, Y., Liu, S., Zhu, L., Seo, S., Richter, A., Li, X., et al. (2023). Global observations of tropospheric bromine monoxide (BrO) columns from TROPOMI. *Journal of Geophysical Research: Atmospheres*, *128*, e2023JD039091. https://doi.org/10.1029/2023JD039091

Received 22 APR 2023
Accepted 30 NOV 2023

Author Contributions:

Conceptualization: Yuyang Chen, Song Liu, Lei Zhu
Data curation: Yuyang Chen, Song Liu
Formal analysis: Yuyang Chen, Song Liu
Funding acquisition: Lei Zhu
Investigation: Yuyang Chen, Song Liu, Sora Seo, Andreas Richter
Methodology: Yuyang Chen, Song Liu
Project Administration: Lei Zhu
Resources: Sora Seo, Andreas Richter, Pieter Valks, Francois Hendrick, Theodore K. Koenig, Rainer Volkamer

Abstract Bromine monoxide (BrO) plays an important role in tropospheric chemistry. The state-of-the-science TROPOspheric Monitoring Instrument (TROPOMI) offers the potential to monitor atmospheric composition with a fine spatial resolution of up to 5.5×3.5 km^2. We present here the retrieval of tropospheric BrO columns from TROPOMI. We implement a stratospheric correction scheme using a climatological approach based on the latest GEOS-Chem High Performance chemical transport model, and improve the tropospheric air mass factor calculation with TROPOMI surface albedo data accounting for the geometrical dependency. Our product presents a good level of consistency in comparison with measurements from ground-based zenith-sky differential optical absorption spectroscopy ($r = 0.67$), aircrafts ($r = 0.46$), and satellites (similar spatial distributions of BrO columns). Furthermore, our retrieval captures BrO enhancements in the polar springtime with values up to 7.8×10^{13} molecules cm^{-2} and identifies small-scale emission sources such as volcanoes and salt marshes. Based on TROPOMI data, we probe a blowing snow aerosol bromine mechanism in which the snow salinity is reduced to better match simulation and observation. Our TROPOMI tropospheric BrO product contributes high-resolution global information to studies investigating atmospheric bromine chemistry.

Plain Language Summary Bromine monoxide (BrO) is an important species that affects the global chemistry of the troposphere. However, global observations of tropospheric BrO remain challenging and limited due to the short lifetime and low abundance. In this study, we present a global high-spatial-resolution tropospheric BrO column product from the TROPOspheric Monitoring Instrument. We describe the retrieval algorithm and present a comprehensive verification and evaluation. In addition, we use the data set to investigate sources and sinks on a daily scale for measurement scenarios of BrO enhancements, such as polar sea ice, volcanic plumes, and salt marshes. We additionally optimize salinity, the key parameter in modeling blow snow aerosol bromine emissions, by comparing simulation and observation. Our work provides unique information to studies exploring atmospheric bromine chemistry.

1. Introduction

Bromine monoxide (BrO) influences global tropospheric chemistry by participating in an autocatalytic chemical cycle that efficiently depletes ozone (Finlayson-Pitts, 2003; Read et al., 2008; Wennberg et al., 1994; von Glasow et al., 2004) and affects the partitioning of HO_x (OH + HO_2) (Simpson et al., 2015). Additionally, the chain reactions impact the atmospheric lifetime of methane (Gilman et al., 2010; Long et al., 2014; Steffen et al., 2006), and the oxidation of dimethyl sulfide (Q. Chen et al., 2018) and elemental mercury (Holmes et al., 2006, 2010;

Software: Yuyang Chen, Song Liu, Xicheng Li, Ao Ding, Wenfu Sun
Supervision: Song Liu, Lei Zhu
Validation: Yuyang Chen, Song Liu, Francois Hendrick, Theodore K. Koenig, Rainer Volkamer
Visualization: Yuyang Chen, Song Liu, Lei Zhu, Sora Seo, Andreas Richter, Xicheng Li, Ao Ding, Wenfu Sun, Lei Shu, Bin Bai, Dakang Wang, Dongchuan Pu, Shuai Sun, Juan Li, Xiaoxing Zuo, Weitao Fu, Yali Li, Peng Zhang, Xin Yang, Tzung-May Fu
Writing – original draft: Yuyang Chen, Song Liu, Lei Zhu
Writing – review & editing: Yuyang Chen, Song Liu, Lei Zhu, Sora Seo, Andreas Richter, Xuan Wang, Pieter Valks, Francois Hendrick, Theodore K. Koenig, Rainer Volkamer

Parrella et al., 2012; Saiz-Lopez et al., 2012; Saiz-Lopez and von Glasow, 2012). However, since BrO is a short-lived radical species (~30 s in the troposphere) with low atmospheric abundance (~1 ppt), observations of tropospheric BrO remain challenging and limited. We develop here a global tropospheric BrO data set making use of high-resolution measurements from the TROPOspheric Monitoring Instrument (TROPOMI) (Veefkind et al., 2012) to provide observational evidence for BrO detection and independent constraints on atmospheric chemistry models.

Tropospheric BrO chemistry is initiated by the formation of reactive inorganic bromine (Br_y = BrO + Br + Br_2 + HOBr + BrCl + IBr + HBr + $BrNO_3$ + $BrNO_2$). Sources of tropospheric Br_y are primarily of natural origins (Schmidt et al., 2016), such as oxidation of bromide from sea salt aerosol (SSA), photolysis and oxidation of very-short-lived organobromines, and transport from the stratosphere (Abrahamsson et al., 2004; Kerkweg et al., 2008; Long et al., 2014; Ordóñez et al., 2012; Saiz-Lopez and von Glasow, 2012; Vogt et al., 1996; von Glasow et al., 2002a, 2002b; Yang et al., 2005, 2019, 2020). During polar springtime, BrO is produced in large quantities in the troposphere from an autocatalytic chain reaction cycle (Barrie & Platt, 1997), known as the "bromine explosion" (Wennberg, 1999), which refers to autocatalytic photochemical and heterogeneous reactions at condensed surfaces, such as sea ice, brine, snowpack, and SSA (Falk & Sinnhuber, 2018; Fan & Jacob, 1992; Huang et al., 2020; Ioannidis et al., 2023; Jeong et al., 2022; Sander & Crutzen, 1996; Sander et al., 2006; Simpson et al., 2007, 2015). Apart from polar regions, localized BrO enhancements are also identified in volcanic plumes (Bobrowski et al., 2003; Choi et al., 2012; Heue et al., 2011; Surl et al., 2015), over salt lakes (Hebestreit et al., 1999; Hönninger et al., 2004; Stutz et al., 2002), and in the marine boundary layer (Badia et al., 2019; Newberg et al., 2005; Sander et al., 2003).

Activation of bromine is hypothesized to take place at the acid surfaces of sulfuric aerosol and SSA, where heterogeneous reactions involve the oxidation of halides by O_3 (R1) to produce HOBr. Then, the uptake of HOBr by aerosols and cloud droplets (Falk & Sinnhuber, 2018; Prados-Roman et al., 2018; X. Wang et al., 2021) produce dihalogens (Br_2 and BrCl) via R2 and R3:

$$Br^- + O_3 + H^+ \rightarrow HOBr + O_2 \quad (R1)$$

$$Br^- + HOBr + H^+ \rightarrow Br_2 + H_2O \quad (R2)$$

$$Cl^- + HOBr + H^+ \rightarrow BrCl + H_2O \quad (R3)$$

Afterward, photolysis of Br_2, BrCl, and HOBr in the troposphere releases bromine radicals (Br·), which react with oxidizers (including O_3) to produce BrO via reactions R4–R7:

$$Br_2 \xrightarrow{h\nu} 2Br\cdot \quad (R4)$$

$$BrCl \xrightarrow{h\nu} Br\cdot + Cl\cdot \quad (R5)$$

$$HOBr \xrightarrow{h\nu} Br\cdot + OH \quad (R6)$$

$$Br\cdot + O_3 \rightarrow O_2 + BrO \quad (R7)$$

An alternative recycling path of BrO involving HO_2 constitutes the ozone destruction mechanism (R6–R8):

$$BrO + HO_2 \rightarrow O_2 + HOBr \quad (R8)$$

Apart from the heterogeneous reactions (R1–R3), bromine within the condensed phase can also be oxidized by gas-phase OH radicals (Abbatt et al., 2012; Frinak & Abbatt, 2006; Sjostedt & Abbatt, 2008) as R9:

$$2OH + 2Br^- \xrightarrow{h\nu} Br_2 + 2OH^- \quad (R9)$$

BrO is commonly used as an observational proxy for total tropospheric reactive bromine. Studies from ground-based platforms confirm extensive BrO enhancements over the polar regions. From in situ measurements, both chemical conversion/resonance fluorescence (Avallone et al., 2003) and chemical ionization mass spectrometry (CIMS) (Liao et al., 2011, 2012) indicate a high correlation between the presence of BrO and loss of surface ozone. Moreover, a significant part of the ground-based monitoring effort has been carried out with differential

optical absorption spectroscopy (DOAS) instruments in remote sensing. Active long-path DOAS and passive zenith-sky DOAS (mainly measuring the stratosphere) and multi-axis DOAS (MAX-DOAS) (probing the vertical structure in the lower troposphere) consistently capture significant BrO enhancements (Hausmann & Platt, 1994; Hendrick et al., 2007; Hönninger et al., 2004; Liao et al., 2011; Peterson et al., 2015; Roscoe et al., 2014; Simpson et al., 2017; Stutz et al., 2011).

In addition to the ground-based data, observations from flight campaigns reveal widespread free-tropospheric BrO. For example, airborne CIMS data during research flights such as Co-ordinated Airborne Studies in the Tropic (Le Breton et al., 2017) and Atmospheric Tomography Mission (ATom) (Veres et al., 2019; Wofsy & ATom Science Team, 2018) identify BrO elevations in the upper free troposphere associated with tropical SSA debromination or organobromines oxidation. Moreover, Airborne MAX-DOAS BrO measurements from CONvective TRansport of Active Species in the Tropics (CONTRAST) (Koenig et al., 2017) and Tropical Ocean tRoposphere Exchange of Reactive halogen species and Oxygenated volatile organic compounds (TORERO) (Volkamer et al., 2015) present a C-shaped BrO profile with peaks in both the boundary layer and the upper free troposphere.

In contrast to ground-based platforms and flight campaigns with high vertical resolution but limited spatial coverage, satellites provide daily global distribution of total and tropospheric BrO columns. For instance, the first tropospheric BrO signals from the Global Ozone Monitoring Experiment (GOME) (Burrows et al., 1999) capture large-scale tropospheric BrO enhancements in the polar springtime (Hollwedel et al., 2004; Platt & Wagner, 1998; Richter et al., 1998). The spaceborne BrO retrievals are extended by a series of polar-orbiting nadir spectrometers, such as the SCanning Imaging Absorption spectrometer for Atmospheric CHartographY (SCIAMACHY) (Bovensmann et al., 1999), Ozone Monitoring Instrument (OMI) (Levelt et al., 2006, 2018), and Global Ozone Monitoring Experiment-2 (GOME-2) (Callies et al., 2000; Munro et al., 2016).

Satellite BrO products have been widely used to identify localized sources from volcanic eruptions or saline lakes (Afe et al., 2004; Hörmann et al., 2016; Suleiman et al., 2019; Theys, van Roozendael, Errera, et al., 2009). BrO products have also improved our understanding of the complex polar bromine chemistry. Specifically, comparisons with model simulations offer implications for snowpack mechanism by optimizing key parameters, such as the age of sea ice (Toyota et al., 2011), base emission rate (Herrmann et al., 2021), and bromine content of the snow (Herrmann et al., 2022). However, the data quality and applications of previous satellite BrO products are limited by spatial resolution (up to 13 km), instrumental issues (e.g., "row anomalies" for OMI), and retrieval accuracy (e.g., out-of-date a priori information).

Here, we present a global high-spatial-resolution tropospheric BrO column product from TROPOMI. Launched in October 2017 onboard the Sentinel-5 Precursor (S-5P) platform, TROPOMI provides nearly daily global coverage with a ∼2,600 km swath width and a ∼13:30 local time (LT) equator crossing time. The spectral resolution is 0.5 nm, and the sampling is 0.2 nm per pixel for the spectral band used in BrO retrieval (McMullan and van der Meulen, 2013). As the successor of the OMI instrument, TROPOMI has an improved signal-to-noise and a spatial resolution of about 5.5×3.5 km^2 (7×3.5 km^2 before 6 August 2019). Following the classical three-step DOAS retrieval, we implement the stratospheric correction scheme using the latest chemical transport model (CTM) simulations with a full halogen (chlorine, bromine, and iodine) chemistry, and we improve the tropospheric air mass factors (AMFs) calculation with TROPOMI surface albedo data accounting for the geometrical dependency.

In Section 2, we give a brief introduction to the Goddard Earth Observing System (GEOS)-Chem CTM. In Section 3, we describe the retrieval algorithm for tropospheric BrO columns. In Section 4, we present the retrieved stratospheric and tropospheric BrO columns, and we compare the TROPOMI results with independent measurements from satellites, ground-based instruments, and flight campaigns. Additionally, we use the data set to investigate sources and sinks for measurement scenarios of BrO enhancements, such as polar sea ice, volcanic plumes, and salt marshes. Finally, we apply the retrieved TROPOMI products to constrain a blowing snow sourced SSA formation mechanism with an improved salinity value.

2. Modeling BrO With the GEOS-Chem Model

Tropospheric bromine chemistry was first added to GEOS-Chem (http://www.geos-chem.org, last access: 15 June 2022) by Parrella et al. (2012), which introduced the oxidant-aerosol chemistry and quantified the effects on tropospheric ozone and mercury budgets. Built on that, Eastham et al. (2014) included a stratospheric bromine

and chlorine scheme; Schmidt et al. (2016) updated the halogen scheme in the troposphere with new heterogeneous reactions; Sherwen et al. (2016) presented a tropospheric iodine-bromine coupling scheme to account for iodine effects on oxidants; Zhu et al. (2019) updated the heterogeneous reactions with a focus on SSA. X. Wang et al. (2019, 2021) adopted these developments for a comprehensive view of tropospheric halogen chemistry in GEOS-Chem with an improved representation of bromine and chlorine chemistry.

Apart from updates on the chemistry mechanism, GEOS-Chem is also under independent development regarding the model framework of the GEOS-Chem High Performance (GCHP) version (https://github.com/geoschem/GCHP, last access: 10 June 2022). To minimize the effects of grid deformation and reduce model bias at high latitudes, GCHP replaces conventional rectilinear latitude-longitude grids with gnomonic cubed sphere grids. By incorporating the classical GEOS-Chem shared-memory code into the Earth System Modeling Framework (ESMF) based framework (MAPL), the efficient GCHP implementation distributes the computation across multiple nodes while retaining high-fidelity global chemical modeling features (Bindle et al., 2021; Eastham et al., 2018).

We use the GCHP version of GEOS-Chem (v13.0.0) with a detailed tropospheric chemistry mechanism for ozon e-organic-VOCs-NO_x-aerosol-halogens (Bey et al., 2001; Schmidt et al., 2016; Sherwen et al., 2016), and the latest updates on the tropospheric halogen chemistry by X. Wang et al. (2019, 2021). Our simulation is based on the NASA Global Modeling and Assimilation Office's Modern-Era Retrospective analysis for Research and Applications, Version 2 (MERRA-2) assimilated meteorological data (Gelaro et al., 2017). The native horizontal resolution of MERRA-2 (0.5° × 0.625°) is degraded to 2° × 2.5° (C48 resolution for GCHP). The vertical resolution is 72 vertical layers. The dynamic time step is 10 min, and the chemical time step is 20 min. We use the Community Emissions Data System (CEDS) inventory for anthropogenic emissions (Hoesly et al., 2018), Model of Emissions of Gases and Aerosols from Nature (MEGAN) (Guenther et al., 2012, 2019) for biogenic emissions, and Global Fire Assimilation System (GFAS) (Kaiser et al., 2012) for fire emissions. We spin up the model for 1 year to ensure species of interest converge at reasonable non-zero levels before running it for 2019 at a temporal resolution of 4 hr. Finally, we sample the model results at the overpass time of TROPOMI.

Figure S1 in Supporting Information S1 shows the global budgets and cycling of reactive bromine species in the troposphere simulated by GCHP. The kinetic and photochemical data compilation utilized in this study is prepared by the NASA Panel for Data Evaluation and incorporated into the standard full chemical mechanism of GEOS-Chem (https://wiki.seas.harvard.edu/geos-chem/index.php/GEOS-Chem_chemistry_mechanisms, last accessed: 1 November 2023). Figure S1 in Supporting Information S1 indicates that $O_3 + Br^-$ is one of the primary initiation steps for the bromine chemistry in the model, alongside $HOCl + Br^-$, $ClNO_3 + Br^-$, $BrNO_3 + Br^-$, $HOI + Br^-$, and $INO_x + Br^-$. The uncertainty in the reaction rate constant k ($O_3 + Br^-$) is 0.1×10^{-12} cm^3 $molecules^{-1}$ s^{-1}, estimated by Ninomiya et al. (2000) based on the cavity ring-down technique. This uncertainty is introduced by a complex heterogeneous multi-step process, and the estimation could be potentially improved by applying the liquid jet X-ray photoelectron spectroscopy technique (Artiglia et al., 2017).

3. Retrieving Tropospheric BrO Columns

We follow the classical three-step DOAS method (Platt & Stutz, 2008; Theys et al., 2011; Theys, van Roozendael, Errera, et al., 2009) to derive the tropospheric BrO vertical column density, V_{tropo}, from TROPOMI as:

$$V_{tropo} = \frac{(S - V_{strato} \times M_{strato})}{M_{tropo}}, \quad (1)$$

where S is the total slant column density, V_{strato} is the stratospheric vertical column density, M_{strato} and M_{tropo} are the stratospheric and tropospheric AMFs, respectively. Figure 1 shows the flowchart of our retrieval approach.

This study uses S from Seo et al. (2019) retrieved with a fitting window of 334.6–358.0 nm, optimized on the basis of sensitivity tests in different measurement conditions. The slant columns show good consistency with GOME-2B (on board the Meteorological Operational satellite B) and OMI satellite products (Pearson correlation coefficient $r = 0.84$) with lower fitting errors and improved detection capability of small-scale hot spots.

3.1. Stratospheric Correction

The stratospheric BrO columns (V_{strato}) are estimated with simulated stratospheric BrO profiles based on a parameterization using dynamical and chemical indicators (Theys, van Roozendael, Errera, et al., 2009). The dynamical impact on the stratospheric BrO distribution is approximated by total ozone columns (inferred by localized

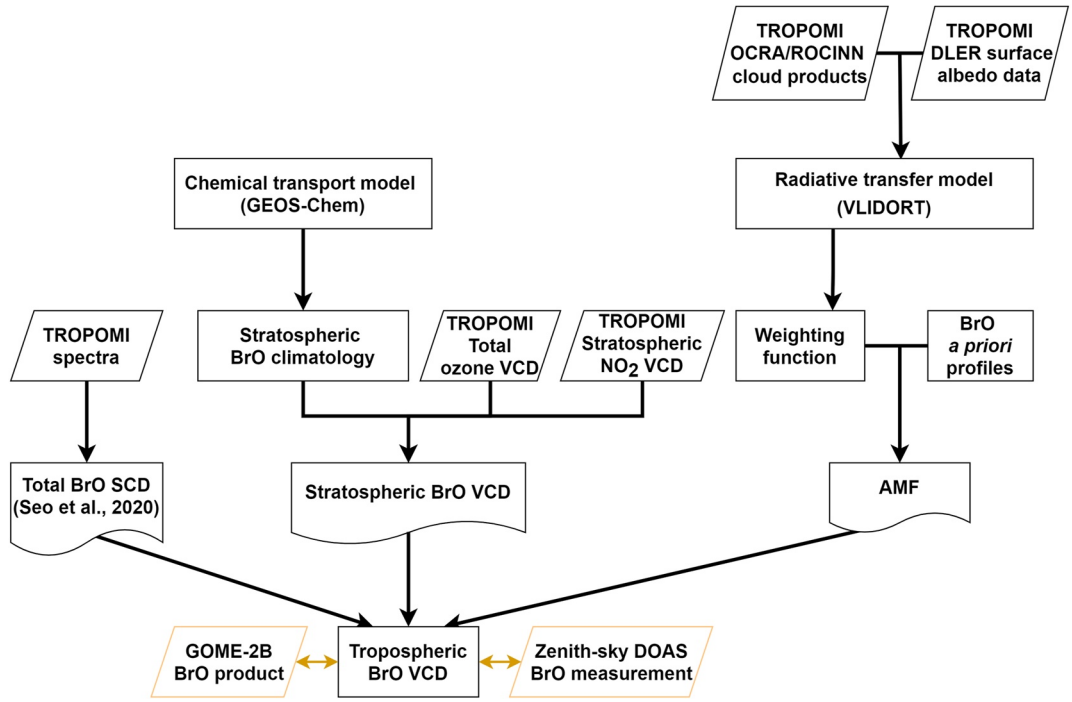

Figure 1. Flow diagram of TROPOspheric Monitoring Instrument (TROPOMI) tropospheric BrO retrieval. A parallelogram represents an input or an output, a rectangle represents a process, and a document symbol represents a product or a model.

Br_y-ozone correlations), while the chemical effect is reflected by stratospheric nitrogen dioxide (NO_2) columns (indicating BrO/Br_y ratio). Comparisons with ground-based, balloon, and spaceborne stratospheric BrO observations suggest that this method is reliable and efficient in separating stratospheric and tropospheric columns (Theys, van Roozendael, Errera, et al., 2009); therefore, it has been applied in previous BrO retrieval studies (e.g., Blechschmidt et al., 2016; Bougoudis et al., 2020; Theys et al., 2011). Note that this method is less satisfactory inside the polar vortex and during ozone-hole conditions (Sihler et al., 2012). For such scenarios, our results show −5% to +25% differences in BrO tropospheric columns, compared to an independent TROPOMI retrieval product using a statistical data analysis for stratospheric correction (Herrmann et al., 2022).

To estimate stratospheric BrO columns, we apply GCHP results in 2019 (Section 2) to construct a look-up table (LUT) containing month, latitude, total ozone column, stratospheric NO_2 column, and solar zenith angle as dimensions. Compared with Theys, van Roozendael, Errera, et al. (2009), our LUT uses an increased number of reference points, such as solar zenith angle (from 5° bins to 3° bins) and latitude (from 10° bins to 3° bins), to reduce interpolation error. For each TROPOMI pixel, a stratospheric BrO profile is interpolated with the LUT using the operational TROPOMI total ozone (Garane et al., 2019) and stratospheric NO_2 (van Geffen et al., 2020) products. The stratospheric BrO column is then derived by integrating the stratospheric BrO profile between the tropopause from MERRA-2 (Gelaro et al., 2017) and the top-of-atmosphere. Here, the upper free tropospheric BrO is assumed to be of stratospheric origin.

3.2. Tropospheric AMF Calculation

The tropospheric AMF (M_{tropo}) is defined as the ratio of the tropospheric slant column density to the tropospheric vertical column density. Assuming BrO as an optically thin atmospheric absorber, we follow Palmer et al. (2001) to calculate M_{tropo} as:

$$M_{\text{tropo}} = \int_{0}^{\text{tropopause}} S(z)w(z)dz, \tag{2}$$

where $S(z)$ represents the shape factor of BrO at altitude z. $w(z)$ denotes the weighting function, computed using the Vector Linearized Discrete Ordinate Radiative Transfer model (version 2.7; Spurr, 2006) at 346 nm and stored

in a LUT as a function of several model inputs, including TROPOMI viewing geometries, surface pressure, and surface albedo. The calculation of M_{strato} relies on the same model parameters as of M_{tropo}, but the dependency on parameters like surface albedo, cloud properties, and a priori BrO profiles is less strong.

Surface albedo is calculated from the TROPOMI directionally dependent Lambertian-equivalent reflectivity (DLER) product (Tilstra, 2022; Tilstra et al., 2021), depending on viewing angles. The TROPOMI DLER product is based on newer observations for 2018–2021 with a higher spatial resolution of 0.125° × 0.125° and an improved treatment of cloud contaminations (Tilstra, 2022), in comparison with the OMI or GOME-2 LER climatologies (Kleipool et al., 2008; Tilstra et al., 2017). Moreover, the TROPOMI DLER extends the isotropic Lambertian assumption with a geometric dependence, which describes the surface anisotropy via a parametrization using the viewing angles and requires no external input of bi-directional reflectance distribution function (Liu et al., 2020, 2021; Tilstra et al., 2021). Compared to the OMI LER climatology, the TROPOMI DLER product shows slightly higher values (<5% over polar regions and <8% over clean Pacific Ocean), which can possibly be related to the degradation of TROPOMI and will be updated with future TROPOMI level-1 data processor (Tilstra, 2022).

In the presence of clouds, we calculate the AMF following the independent pixel approximation (R. V. Martin et al., 2002), which defines the AMF as a linear combination of a fully cloudy scene and a clear scene weighted by cloud fraction. We adopt cloud properties from the TROPOMI operational cloud products based on the Optical Cloud Recognition Algorithm (OCRA) and Retrieval Of Cloud Information using Neural Networks (ROCINN) algorithms (Loyola et al., 2018, 2020; Lutz et al., 2016). The TROPOMI OCRA/ROCINN products have been widely used for cloud correction in TROPOMI trace gas retrievals, such as ozone (Heue, Eichmann, & Valks, et al., 2021; Heue, Spurr, et al., 2021), sulfur dioxide (SO_2) (Theys et al., 2017), formaldehyde (HCHO) (De Smedt et al., 2018), and NO_2 (Liu et al., 2021). OCRA/ROCINN apply snow and ice masks to determine snow- and ice-covered scenes. However, such high reflective surfaces are in general a particular challenge for cloud algorithms (Latsch et al., 2022) Differences among current TROPOMI cloud products and impacts on our BrO retrieval will be investigated in the near future.

For the shape factor $S(z)$, we assume a constant tropospheric BrO profile in the first km for high surface albedo (larger than 0.5) and a Gaussian profile with a maximum at 6 km and a full-width half maximum of 2 km for low surface albedo (smaller than 0.5), following Theys et al. (2011). This hypothetical BrO profile is broadly in line with balloon observations in the Arctic (Fitzenberger et al., 2000).

In the following analysis, we filter out pixels with cloud fraction larger than 0.4, difference between the surface pressure and the cloud pressure larger than 400 hPa, solar zenith angle larger than 75°, and tropospheric AMF (normalized by geometric AMF) lower than 0.2. We regrid level-2 BrO pixels onto a spatial resolution of 0.5° × 0.5° for monthly data using the oversampling technique from our previous studies (Zhu et al., 2014, 2017), and we show daily examples using the original resolutions of satellites.

3.3. Error Budget of the Retrieved Tropospheric BrO Columns

We consider three main sources of errors in the retrieval algorithm, including (a) measurement noise and spectral fitting errors during the slant column fitting, (b) errors in separating stratospheric and tropospheric BrO, and (c) systematic errors due to uncertainties in model parameters affecting the tropospheric AMF. We use error propagation (Boersma et al., 2004; De Smedt et al., 2008, 2018; Theys et al., 2011) to derive the total error on the tropospheric vertical columns ($\sigma_{V_{\text{tropo}}}$) as:

$$\sigma^2_{V_{\text{tropo}}} = \frac{1}{N} \cdot \left(\frac{\sigma_{S_{\text{rand}}}}{M_{\text{tropo}}}\right)^2 + \left(\frac{\sigma_{S_{\text{syst}}}}{M_{\text{tropo}}}\right)^2 + \left(\frac{\sigma_{S_{\text{strato}}}}{M_{\text{tropo}}}\right)^2 + \left(\frac{(S - S_{\text{strato}}) \cdot \sigma_{M_{\text{tropo}}}}{M^2_{\text{tropo}}}\right)^2, \tag{3}$$

where $\sigma_{S_{\text{rand}}}$ and $\sigma_{S_{\text{syst}}}$ are respectively the random (instrumental noise) and systematic (selection of the physical model and reference spectra) error on the slant columns. N is the number of ground pixels. $\sigma_{S_{\text{strato}}}$ and $\sigma_{M_{\text{tropo}}}$ stand for the errors on the stratospheric slant column and the tropospheric AMF, respectively.

$\sigma_{M_{\text{tropo}}}$ is derived from individual input parameters (Boersma et al., 2004; De Smedt et al., 2008, 2018) as:

$$\sigma^2_{M_{\text{tropo}}} = \left(\frac{\partial_{M_{\text{tropo}}}}{\partial_{A_s}} \cdot \sigma_{A_s}\right)^2 + \left(\frac{\partial_{M_{\text{tropo}}}}{\partial_{f_c}} \cdot \sigma_{f_c}\right)^2 + \left(\frac{\partial_{M_{\text{tropo}}}}{\partial_{P_{\text{cloud}}}} \cdot \sigma_{P_{\text{cloud}}}\right)^2 + \left(\frac{\partial_{M_{\text{tropo}}}}{\partial_S} \cdot \sigma_S\right)^2, \tag{4}$$

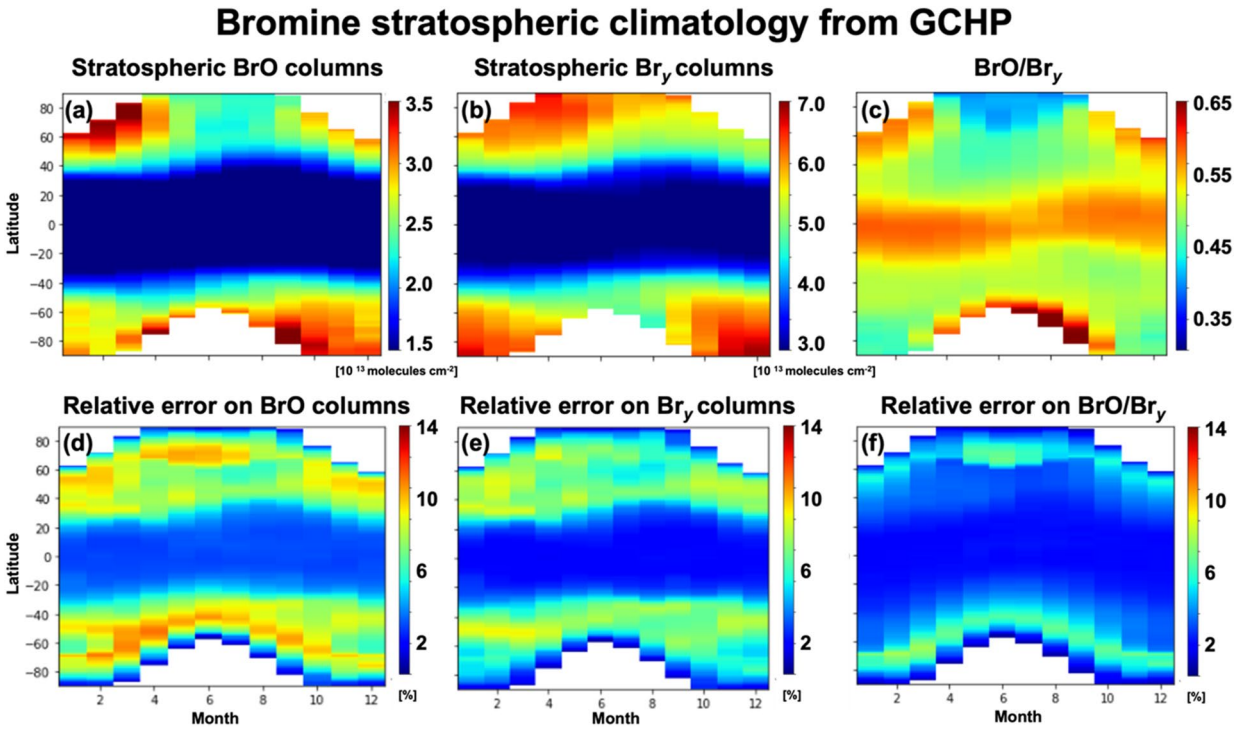

Figure 2. Monthly and zonal averaged stratospheric BrO columns from the GEOS-Chem high performance (GCHP) simulations (a) along with the associated dynamical (stratospheric Br$_y$ columns; b) and chemical (BrO/Br$_y$) parameterization (c). Relative error (defined by the ratio of standard deviation to mean) for stratospheric BrO columns (d), dynamical indicator (e), and chemical indicators (f) are also shown.

where $\frac{\partial_{M_{\text{tropo}}}}{\partial_{\text{parameter}}}$ is the AMF derivative, and σ_{A_s}, σ_{f_c}, $\sigma_{P_{\text{cloud}}}$, and σ_S are typical uncertainties on the surface albedo, cloud fraction, cloud top pressure, and profile shape, respectively, assessed from the literature or inferred by comparing with independent data. The typical uncertainties are 0.027 for DLER albedo (Tilstra, 2022; Tilstra et al., 2021), 0.05 for the OCRA cloud fraction, and 50 hPa for ROCINN cloud pressure (Loyola et al., 2020).

Overall, the retrieval error on monthly averaged tropospheric BrO columns $\left(\sigma_{V_{\text{tropo}}}\right)$ is <70%. For the slant column, $\sigma_{S_{\text{rand}}}$ is 5×10^{13} molecules cm^{-2}, estimated following a statistical method (Boersma et al., 2007) and $\sigma_{S_{\text{syst}}}$ is <10%, following Seo et al. (2019). For stratospheric columns, $\sigma_{S_{\text{strato}}}$ is <20%, derived from the comparison with ground-based measurements (Section 4.3). The overall error of the tropospheric AMF $\left(\sigma_{M_{\text{tropo}}}\right)$ is <60%, with $\left[\frac{\partial_{M_{\text{tropo}}}}{\partial_{\text{parameter}}} \cdot \sigma_{\text{parameter}}\right] < 20\%$ for surface albedo, <15% for cloud fraction, <20% for cloud-top height, and <50% for the profile shape.

4. Results and Discussion

4.1. Stratospheric Correction

Figure 2 shows the stratospheric BrO climatology from GCHP simulations at TROPOMI overpass time. Elevated stratospheric BrO and Br$_y$ (i.e., dynamical indicator) columns are observed for middle and high latitudes due to lower tropopause height. For the BrO/Br$_y$ ratio (i.e., chemical indicator), higher values at low latitudes are related to low Br$_y$ from Br$_y$/ozone correlations. Furthermore, seasonal variations for the BrO/Br$_y$ ratio are stronger in middle and high latitudes, primarily due to the natural variations in stratospheric NO_2. These seasonal and latitudinal dependencies are broadly consistent with the Belgian Assimilation System for Chemical Observations from Envisat CTM (Viscardy et al., 2010) climatology from Theys, van Roozendael, Errera, et al. (2009) designed for satellites with morning overpasses (GOME, SCIAMACHY, and GOME-2) (Figure 13 therein). However, our climatology result is generally 10% lower than that of Theys, van Roozendael, Errera, et al. (2009), reflecting the differences in simulation period (2003–2006 for Theys, van Roozendael, Errera, et al., 2009), overpass time (9:30 LT for GOME-2), and chemistry scheme.

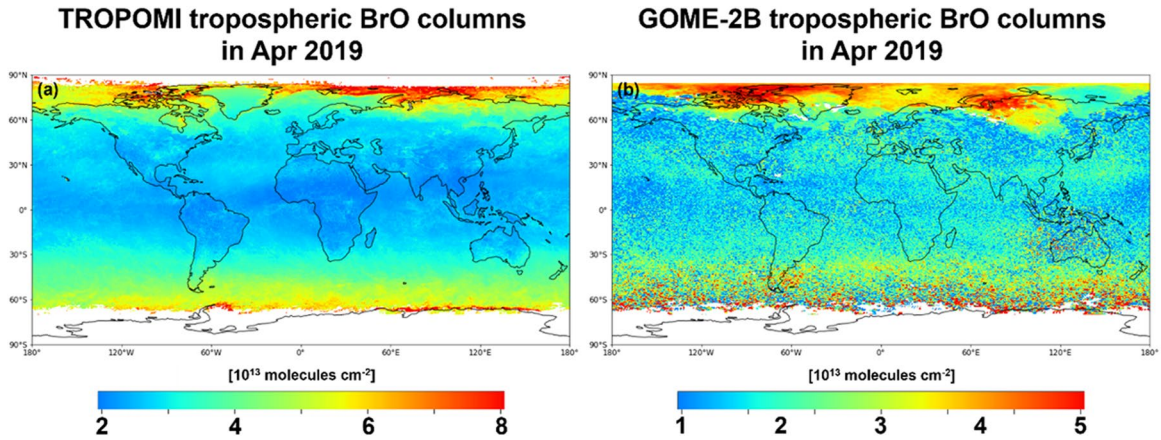

Figure 3. Monthly mean tropospheric BrO columns retrieved from TROPOspheric Monitoring Instrument (TROPOMI) (a; this study) and GOME-2B (b; Theys et al., 2011) in April 2019. Note that the two panels are with different color bars.

Figure 2 also shows the relative uncertainties on the stratospheric BrO columns and the contributions from the Br_y and BrO/Br_y parameterizations, which are calculated from the GCHP model variability. The uncertainties on the stratospheric BrO columns are dominated by Br_y, with high values in middle and high latitudes during the winter and spring months. For these scenarios with strong variations in both dynamics and chemistry, increased proportions for BrO/Br_y uncertainties are also noticed. The relative uncertainties for BrO are typically <11%, with uncertainty <10% for Br_y and <8% for BrO/Br_y.

4.2. Global Distribution of Tropospheric BrO Columns

Figure 3 compares the global distribution of monthly average tropospheric BrO columns from our TROPOMI retrieval and the GOME-2B product in April 2019. Both satellite products highlight elevated BrO columns (higher than 5.0×10^{13} molecules cm^{-2}) over the Arctic sea ice and snow regions, as captured in earlier satellite observations (Begoin et al., 2010; Blechschmidt et al., 2016; Richter et al., 2002; Simpson et al., 2007; Zhao et al., 2016) but higher than in situ studies ($\sim 1.8 \times 10^{13}$ molecules cm^{-2}) (Liao et al., 2012; Neuman et al., 2010; Peterson et al., 2015, 2017, 2019) and DOAS observations (Peterson, Pratt, et al., 2016; Peterson, Simpson, & Nghiem, 2016; Peterson et al., 2017, 2018; Simpson et al., 2017). We find low BrO columns of $\sim 2.2 \times 10^{13}$ molecules cm^{-2} in the tropical and subtropical regions, where BrO columns are primarily from SSA debromination (R1 and R2) and organobromines oxidation (Sherwen et al., 2016; Simpson et al., 2015; Zhu et al., 2019). Compared with GOME-2B, TROPOMI provides higher tropospheric BrO columns and lower noise, likely due to the different spatial resolution (80×40 km^2 for GOME-2), overpass time (9:30 LT for GOME-2), and retrieval algorithm (Theys, van Roozendael, Errera, et al., 2009; Theys et al., 2011). The generally reduced noise from TROPOMI indicates improved data quality and lower DOAS fitting residuals. The larger BrO differences in polar regions mostly reflect the differences in stratospheric correction and/or AMF calculation.

Figure S2 in Supporting Information S1 shows the simulated global distribution of monthly mean tropospheric BrO in April 2019, which is broadly consistent with satellite measurements in Figure 1 regarding the BrO spatial distribution. However, GCHP underestimates tropospheric BrO columns by ~75% in polar regions, possibly due to the missing SSA emission mechanisms over sea-ice-covered areas, such as blowing snow or first-/multi-year sea ice. Please refer to Section 4.5 for additional discussions regarding polar bromine sources.

Figure 4 shows the total (slant columns normalized by geometric AMF), stratospheric, and tropospheric BrO columns, and corresponding tropopause height in the Northern Hemisphere from 11–13 April 2019, a designated period with high-BrO events in the Arctic spring. The pattern of stratospheric BrO columns broadly anticorrelates with that of tropopause heights, supporting that the stratospheric correction properly accounts for changes in tropopause heights by using total ozone columns as indicators. The stratospheric BrO columns can be underestimated for particularly low tropopause heights of ~6 km, likely due to the transport of stratospheric BrO into the free troposphere or the retrieval uncertainty in the stratospheric correction (Salawitch et al., 2010; Theys et al., 2011). The tropospheric BrO hotspots may originate mainly from precursor emissions over the ice- or snow-cover surface, as shown in Figure 3.

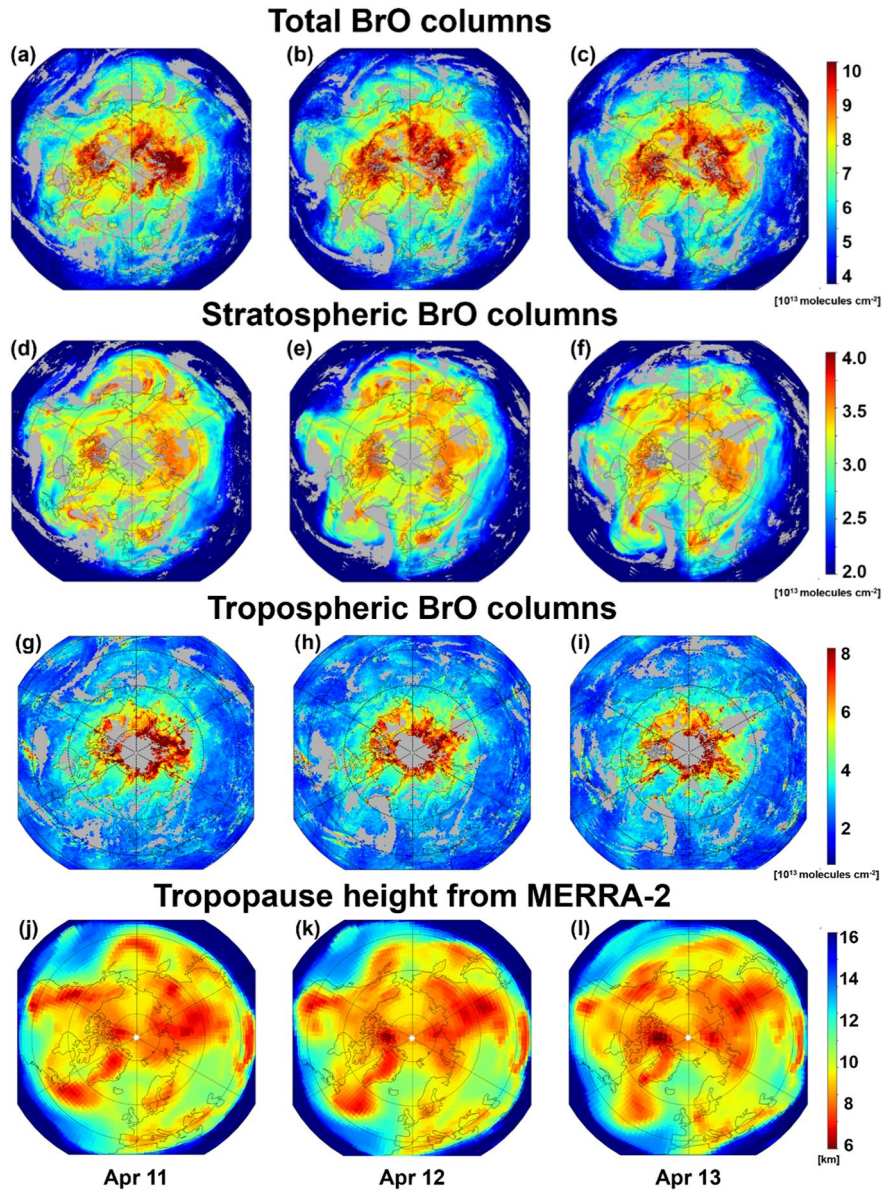

Figure 4. Total (a–c), stratospheric (d–f), and tropospheric (g–i) BrO columns from TROPOspheric Monitoring Instrument (TROPOMI) and tropopause height from Modern-Era Retrospective analysis for Research and Applications, Version 2 (MERRA-2) (j–l). Results are presented for 11, 12, and 13 in April 2019 in the Northern Hemisphere (30°–90°N).

Figure 5 shows the monthly variations in TROPOMI tropospheric BrO columns over the polar regions during the spring of 2019. At the beginning of the spring, pronounced tropospheric BrO columns are likely due to the bromine explosion after the polar night, according to the simulation. In this process, heterogeneous reactions release Br_2 and BrCl into the gas phase and contribute the BrO catalytically from the condensed phase (liquid brine or sea ice). In the following months, BrO values decline gradually as the wet deposition of HBr begins to dominate the sink of Br_y (Zhu et al., 2019). Such a seasonality in BrO columns is similarly captured by GOME, OMI, and GOME-2 (e.g., Begoin et al., 2010; Levelt et al., 2006; Platt & Wagner, 1998; Richter et al., 1998; Theys et al., 2011). The spatial variations of BrO values may reflect the heterogeneous reactions on sea ice, including the first-year sea ice (Bougoudis et al., 2020) and the multi-year ice (Herrmann et al., 2022). The discrepancy of BrO distribution between the northern and southern hemisphere can be additionally influenced under ozone-hole conditions.

Figure 6 shows the seasonal cycle of the retrieved TROPOMI tropospheric BrO columns. Figure S3 in Supporting Information S1 shows the global distribution of monthly mean BrO columns in 2019. Generally, the seasonal

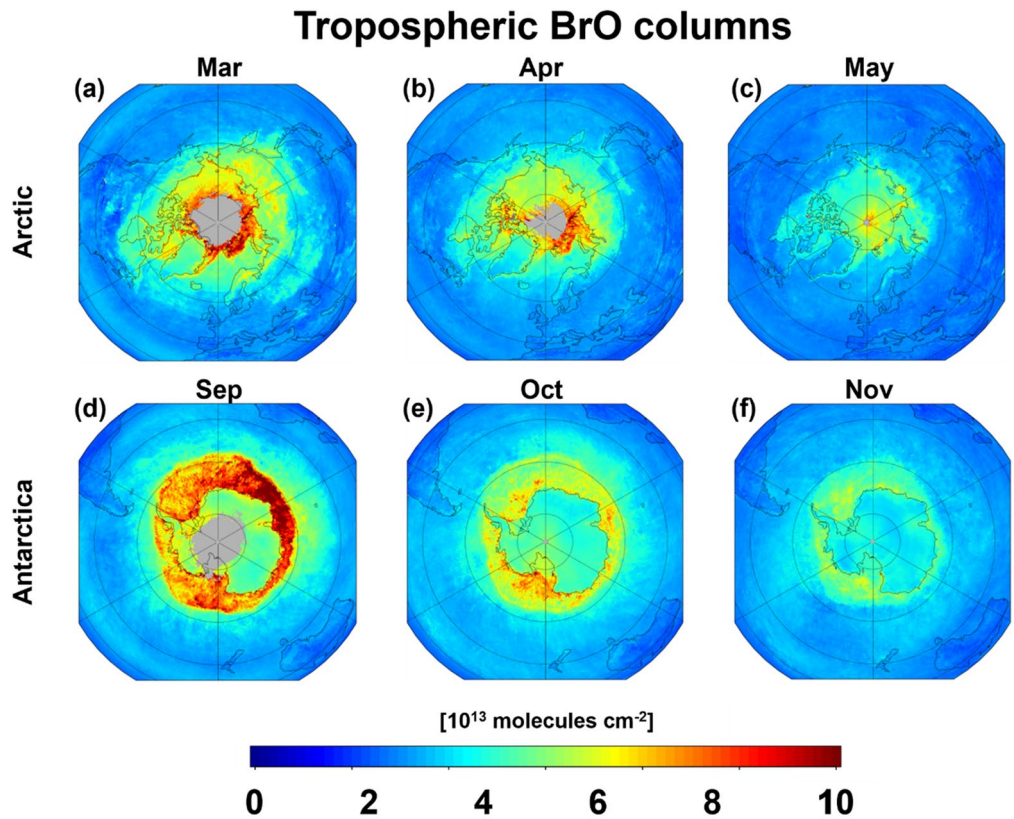

Figure 5. Monthly mean TROPOspheric Monitoring Instrument (TROPOMI) tropospheric BrO columns in polar spring 2019 in the Northern Hemisphere (30°–90°N) (a–c) and the Southern Hemisphere (30°–90°S) (d–f).

variations are weak for middle and low latitudes, with the tropospheric BrO values in the range of 2.4×10^{13} molecules cm^{-2} to 4.3×10^{13} molecules cm^{-2}. Tropospheric BrO columns show stronger variations at high latitudinal bands, especially in the springtime. In the polar spring, for example, monthly mean tropospheric BrO columns can reach 7.8×10^{13} molecules cm^{-2}, likely originating from heterogeneous bromine activation from natural sources (Richter et al., 2011), including sea ice (Choi et al., 2018; Yang et al., 2020), snowpack (Custard et al., 2017; Peterson et al., 2018; Pratt et al., 2013), and SSA from blowing snow (Blechschmidt et al., 2016; Domine et al., 2004; Frey et al., 2020; Yang et al., 2008). The standard deviations are 0.3×10^{13} molecules cm^{-2} to 0.9×10^{13} molecules cm^{-2} in summer and 0.4×10^{13} molecules cm^{-2} to 2.4×10^{13} molecules cm^{-2} in winter.

4.3. Evaluation With Remote Sensing BrO Measurements

Figure 6 also compares TROPOMI tropospheric BrO columns with MAX-DOAS measurements from the TORERO (eastern tropical Pacific during January–February 2012; Volkamer et al., 2015) and CONTRAST (western tropical Pacific during January–February 2014; Koenig et al., 2017) aircraft campaigns. TROPOMI tropospheric BrO columns are generally higher than the TORERO MAX-DOAS results by up to $\sim 1.0 \times 10^{13}$ molecules cm^{-2}, likely due to retrieval errors, differences in the observation periods, and sensitivities of columns to BrO vertical profiles (satellite measurements present low sensitivity in the lower atmosphere; Koenig et al., 2017; Liu et al., 2019, 2020; Verhoelst et al., 2021).

Figure 7 compares the tropospheric BrO columns from TROPOMI and TORERO aircraft campaigns over the tropical Pacific in February, acknowledging the inter-annual variability between 2012 and 2019. The TROPOMI BrO values along the flight tracks vary from 2.0×10^{13} molecules cm^{-2} to 3.1×10^{13} molecules cm^{-2}, consistent with the airborne MAX-DOAS measurements. Upon eliminating a background tropospheric BrO level of 1.2×10^{13} molecules cm^{-2} (~1 ppt; Neuman et al., 2010), we observe a correlation coefficient $r = 0.46$ (Figure S4 in Supporting Information S1). The discrepancy of $\sim 1.3 \times 10^{13}$ molecules cm^{-2} between campaigns and

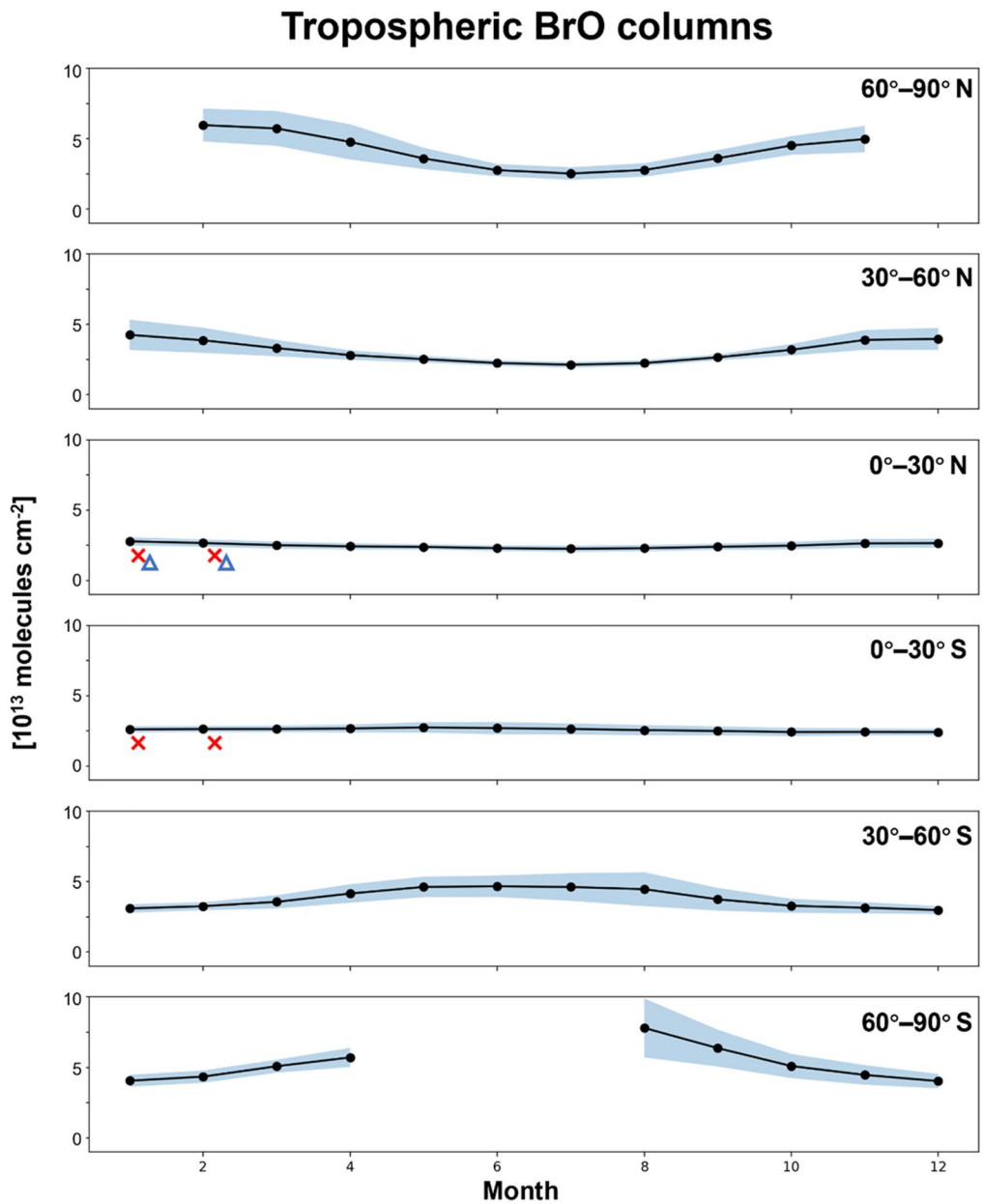

Figure 6. Monthly averaged tropospheric BrO columns in 2019 from different latitude bands. The shaded area represents the standard deviation, defined from BrO columns within each latitude band for a given month. Red crosses (1.8×10^{13} molecules cm^{-2}) and blue triangles (1.6×10^{13} molecules cm^{-2}) represent tropospheric BrO columns averaged for the TORERO aircraft campaign (Volkamer et al., 2015; Dix et al., 2016; above the eastern tropical Pacific Ocean) and the CONvective TRansport of Active Species in the Tropics campaign (Koenig et al., 2017; over the western tropical Pacific Ocean), respectively. Measurements from aircraft campaigns are calculated by integrating profiles over the altitude range of the aircraft and horizontally shifted in the figure for presentation purposes.

satellite measurements is possibly due to the reduced SSA emissions in summer, the reduced detection sensitivity of tropospheric BrO in the free troposphere by MAX-DOAS measurements, and imperfect stratospheric correction in the satellite retrieval. Both TROPOMI and TORERO show higher BrO columns located far from the coastline in mid-latitudes, while the inland BrO amounts are close to the background values. This land-ocean contrast likely results from (a) SSA mass difference, with fine component dominating the SSA mass over land, for which the SSA debromination is more intensive (Zhu et al., 2019); (b) reduced bromine inputs to terrestrial convection, since the surface influx does not connect with bromine sources (primarily marine in their origin);

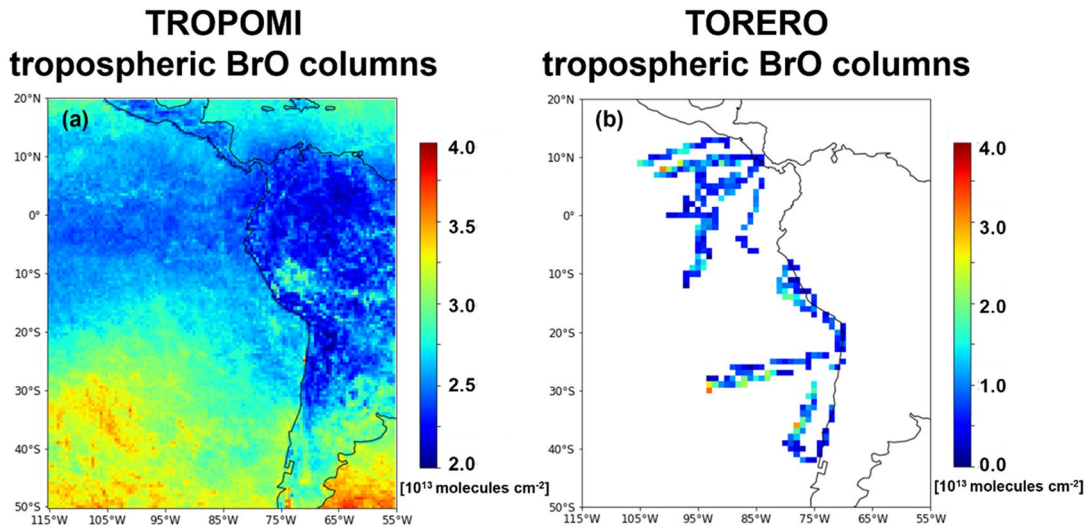

Figure 7. Tropospheric BrO columns retrieved from TROPOspheric Monitoring Instrument (TROPOMI) in February 2019 (a) and measured during the TORERO aircraft campaign (Volkamer et al., 2015) in February 2012 (b) over the tropical Pacific Ocean. TORERO observations are displayed along the flight track.

and (c) increased wash-out of bromine aloft by wet scavenging, since terrestrial convection is increased (Schmidt et al., 2016; Volkamer et al., 2015; S. Wang et al., 2015).

Figure 8 compares the tropospheric BrO data from TROPOMI, GOME-2B, and ground-based instruments. The ground-based data are from zenith-sky DOAS measurements over Harestua, Norway (60.22°N, 10.75°E), a station operated by BIRA-IASB as part of the Network for the Detection of Atmospheric Composition Change (Hendrick et al., 2007). Figure S5 in Supporting Information S1 additionally shows tropospheric BrO columns from the MAX-DOAS instrument during springtime from 2012 to 2016 at Utqiagvik, Alaska (71.33°N, 156.67°W) (Peterson et al., 2015; Simpson et al., 2017, 2018). We average the TROPOMI and GOME-2B pixels within a 50 and 200 km radius, respectively, from the location of the DOAS instrument for each day (Theys et al., 2011), and we average the ground-based measurements within ±1 hr of the TROPOMI overpass time (13:30 LT). A scaling factor of 1.2, estimated using the 2019 GCHP simulations (Section 2), is additionally applied to GOME-2B measurements to correct the BrO diurnal variation caused by different overpass times.

In Figure 8, space-based and ground-based data show differences in tropospheric BrO columns on an average of 1.9×10^{13} molecules cm^{-2}. A systematic overestimation of TROPOMI tropospheric BrO columns is observed particularly in wintertime with large solar zenith angles, ranging from 0.2×10^{13} molecules cm^{-2} to 4.6×10^{13} molecules cm^{-2}. This results from the low sensitivity of zenith-sky DOAS instruments close to the surface (Roscoe et al., 2014). With higher sensitivity in the lower troposphere, the MAX-DOAS measurements present increased daily variations, for example, in April–May 2013. The difference in tropospheric BrO columns between TROPOMI and MAX-DOAS is, on average, 0.8×10^{13} molecules cm^{-2}. In general, our TROPOMI

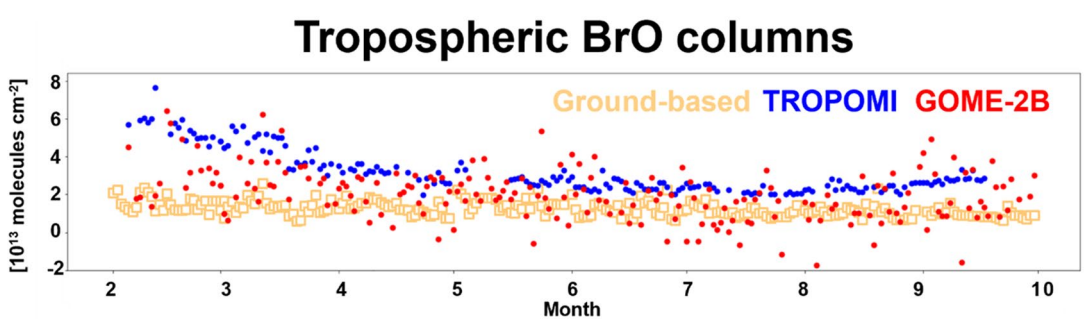

Figure 8. Tropospheric BrO columns from TROPOspheric Monitoring Instrument (TROPOMI) and ground-based zenith-sky differential optical absorption spectroscopy instrument at Harestua (60.22°N, 10.75°E) in February–October 2019. Tropospheric BrO columns from GOME-2B are also shown, with a scaling factor of 1.2 applied to address the diurnal variations of BrO at different overpass times.

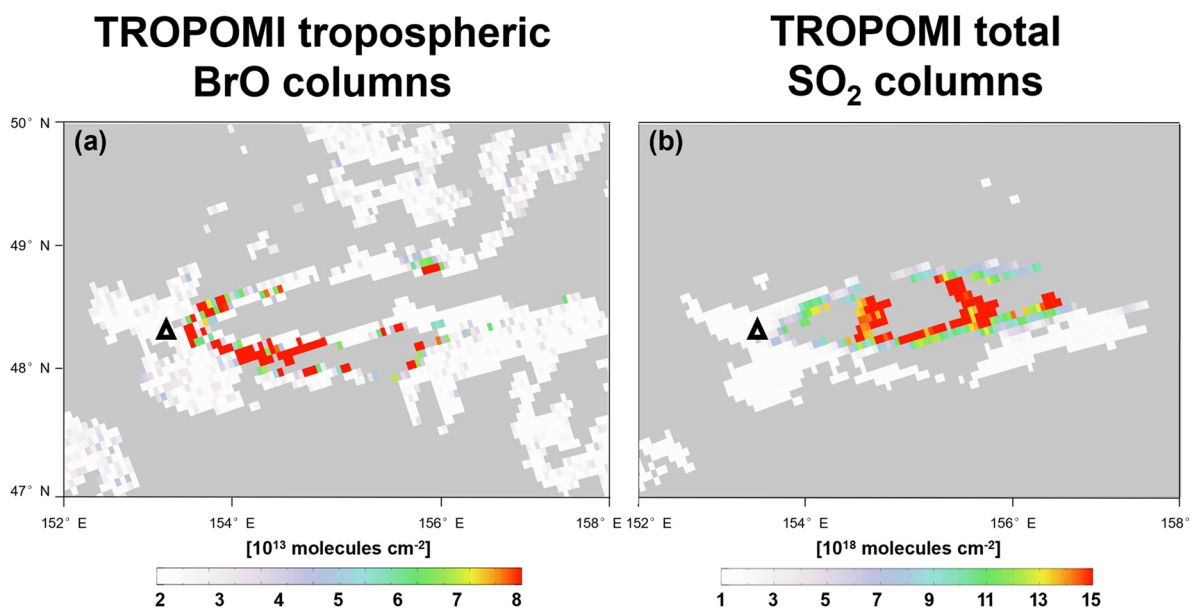

Figure 9. TROPOspheric Monitoring Instrument (TROPOMI) tropospheric BrO (a) and total SO_2 (b) columns over the Raikoke volcano (48.29°N, 153.25°E) on the Kuril Islands after the eruption on 21–22 June 2019. TROPOMI total SO_2 columns are calculated assuming plume heights of 6.5–7.5 km (mid-troposphere). The open triangle marks the volcano's location.

retrieval shows improved consistency with ground-based measurements ($r = 0.67$ for zenith-sky DOAS data, Figure S6 in Supporting Information S1), in comparison with GOME-2B ($r = 0.28$, not shown).

4.4. Tropospheric BrO Hotspots According to TROPOMI

Explosive volcanic eruptions typically emit a large amount of ash and reactive gases. In the vicinity of volcanic activities, high-temperature gas-phase reactions and in-plume heterogeneous chemical processes involving aerosols during plume transport lead to high mixing ratios of BrO. The high temperature increases the concentration of HOBr and accelerates the catalytic cycles (R2), thereby enhancing the production of Br· and BrO (R4 and R7) on the acidic surface of sulfuric aerosols (Gutmann et al., 2018; R. S. Martin et al., 2009; Oppenheimer et al., 2006; von Glasow, 2010). The high level of BrO in the downwind region is similarly captured by OMI and GOME-2 studies (Choi et al., 2012; Heue et al., 2011; Theys, van Roozendael, Dils, et al., 2009). In Figure 9, our TROPOMI tropospheric BrO retrievals report significantly enhanced BrO values from the volcanic eruption at Raikoke (48.29°N, 153.25°E) from 21–22 June 2019, ranging from 6.5×10^{13} molecules cm^{-2} to 8.0×10^{13} molecules cm^{-2}.

To distinguish between the plume chemistry and the dilution effects, bromine species are usually reported relative to sulfur (McGonigle et al., 2004; von Glasow et al., 2009). Specifically, SO_2 is regarded as an optical plume tracer for observing volcanic eruptions, because its concentration is not significantly affected by the acidity of the volcanic aerosol or by reactions with other oxidants, and it remains relatively stable in the volcanic plume over short time scales (minutes to hours). TROPOMI captures the large plume of BrO transported toward the southeast, with a similar evolution pattern reflected by the TROPOMI SO_2 product (Hedelt et al., 2019). Our estimation of the BrO/SO_2 ratio is $\sim 0.9 \times 10^{-5}$, which falls within the range of 1.0×10^{-6} to 1.0×10^{-3} in volcanic plumes, compiled by Gutmann et al. (2018) (and references therein).

Salt marshes, with facilitated heterogeneous reactions that emit Br_2 and BrCl into the gas phase, are among the most localized and strongest sources of tropospheric BrO (Saiz-Lopez and von Glasow, 2012). Ground-based DOAS instruments observe high BrO concentrations up to 86 ppt over the Dead Sea (Hebestreit et al., 1999; Matveev et al., 2001; Tas et al., 2005), the Great Salt Lake (Stutz et al., 2002), and Salar de Uyuni (Hönninger et al., 2004). OMI and GOME-2 measurements reveal high BrO columns of up to 1.4×10^{14} molecules cm^{-2} for salt deserts over the Great Salt Lake (Chance, 2006) and the Rann of Kutch (Hörmann et al., 2016). Our TROPOMI retrieval captures BrO enhancements for a selected salt marsh, the Rann of Kutch in India and

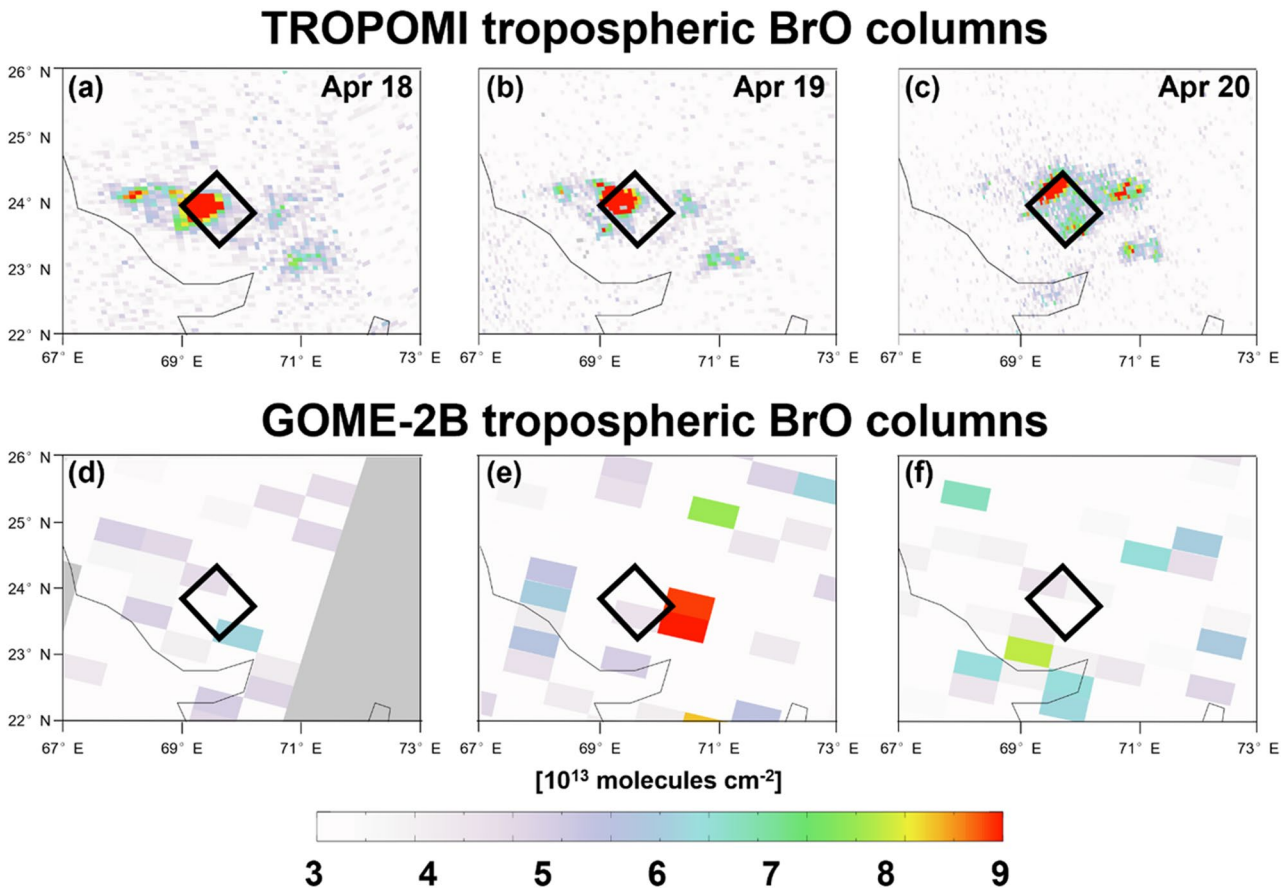

Figure 10. Tropospheric BrO columns from TROPOspheric Monitoring Instrument (TROPOMI) (a–c) and GOME-2 (d–f) over the Rann of Kutch salt marsh (24.02°N, 70.14°E) on 18–20 April 2019. The rectangle marks the salt marsh location.

Pakistan, one of the most substantial natural sources of reactive bromine compounds (Hörmann et al., 2016; Seo et al., 2019). In Figure 10, TROPOMI retrieval from 18 to 20 April 2019, shows distinguished BrO plumes by up to $\sim 1.1 \times 10^{14}$ molecules cm^{-2} with significantly more spatial details than the GOME-2B data sets, highlighting the ability of TROPOMI to observe small-scale BrO enhancements.

4.5. Implications for Testing Blowing Snow Aerosol Bromine Mechanism

Salinity is one of the most critical parameters in the blowing snow mechanism in model simulations (Yang et al., 2008, 2010). Arctic snow salinity has been reported by field studies to exhibit a large variability, approximately ranging from ~0 to 20 practical salinity units (psu) (Krnavek et al., 2012; Nomura et al., 2018; Peterson et al., 2018; Tonboe et al., 2021). Current models typically apply a uniform snow salinity, that is, 0.1 psu for the first-year sea ice and 0.05 psu for the multi-year sea ice, over sea ice for the Arctic (Huang et al., 2018, 2020; Huang & Jaeglé, 2017; Marelle et al., 2021; Swanson et al., 2022). To improve our understanding of the impact of salinity in models, we compare the retrieved TROPOMI product to model simulations with different snow salinity values over sea ice (first-year sea ice: 0.01, 0.05, 0.1, 2 psu; multi-year sea ice: half of the snow salinity over first-year sea ice). Our simulation incorporates a representation of snowpack Br_2 production from Toyota et al. (2011), where Br_2 is emitted upon deposition of precursor species HOBr, $BrNO_3$, and ozone in snowpacks with adequate salinity, acidity, and depth. Specific chemical equations of Br_2 emissions from the sunlit snowpack surface are nevertheless limited (as shown in Figure S1 in Supporting Information S1). Additionally, we also add a blowing snow SSA production mechanism, which increases aerosol particulate bromide and thus facilitating heterogeneous recycling of reactive bromine on aerosol surfaces (Huang et al., 2018, 2020; Swanson et al., 2022). We acknowledge that multiphase reactions on the surface and snowpack photochemistry, for example, OH radical oxidation of Br^- to produce Br_2 (Halfacre et al., 2019), are not explicitly represented in the current setup, so

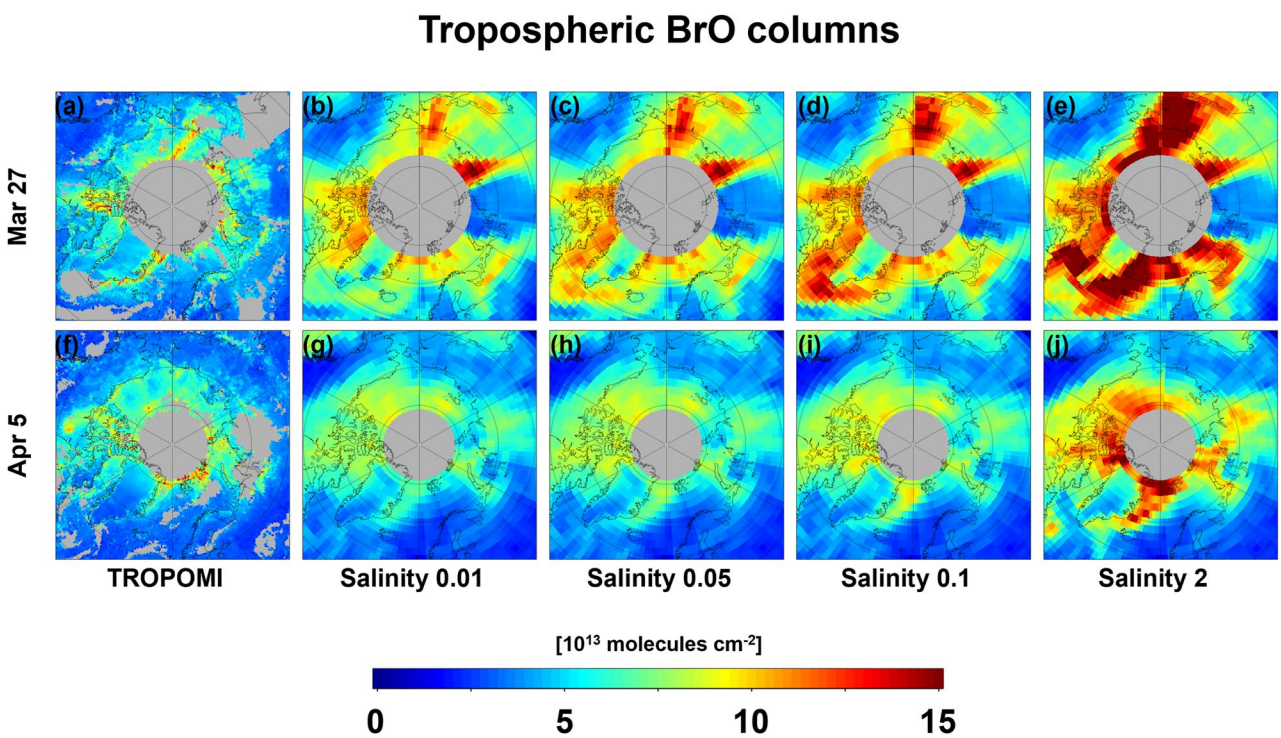

Figure 11. Tropospheric BrO columns from TROPOspheric Monitoring Instrument (TROPOMI) observations and model simulations with different salinity of snow (in practical salinity units) on 27 March (a–e) and 5 April (f–j) in 2019 in the Northern Hemisphere (60°–90°N).

that approximated parameterization of the release of Br_2 may introduce uncertainty into the simulation results. We apply the satellite averaging kernels to the modeled vertical profiles to remove errors resulting from a priori profile assumptions, and we interpolate the model outputs to TROPOMI overpass time.

Figure 11 presents the tropospheric BrO columns from TROPOMI and model simulations utilizing different snow salinity values in the blowing snow scheme. On 27 March (Figures 11a–11e), the TROPOMI products and all simulations capture the high values of tropospheric BrO columns over the Chukchi Sea, Canadian Arctic Archipelago, East coast of Greenland island, and East Siberian Sea. However, the use of relatively high snow salinity (0.05, 0.1, and 2 psu over first-year sea ice) leads to large BrO enhancements over Greenland island and the seas around it, likely due to an overestimation of SSA production by the blowing snow scheme. Overall, the simulation with a reduced salinity (0.01 psu) achieves the best agreement with TROPOMI, with a bias of $\sim 2.3 \times 10^{13}$ molecules cm^{-2}. A similar conclusion can be drawn for 5 April (Figures 11f–11j), where using a salinity of 0.01 improves the consistency with TROPOMI particularly over the Canadian Arctic Archipelago and east of the coast of Greenland.

Reducing the salinity does not remove all disagreements with satellite data. For both days, the modeled BrO is overestimated over the Chukchi Sea and the east coast of Greenland island. Additionally, the model (even with a salinity of 0.01 psu) frequently shows BrO enhancements where the satellite doesn't observe such changes, especially around Hudson Bay and Baffin Bay. These discrepancies suggest future investigations of additional key parameters affecting SSA generation in blowing snow schemes, such as humidity, temperature, wind speed, or snow particle size distribution. Our new TROPOMI BrO product provides independent indirect constraints on testing new chemistry schemes or critical parameters.

5. Conclusions

We retrieve tropospheric BrO columns from the TROPOMI on the European S-5P platform. The retrieved BrO data is essential in exploring the chain reactions of bromine species and quantifying their impact on atmospheric oxidizing capacity. We implement a stratospheric correction scheme using a climatological approach based on the GCHP CTM. The model is equipped with a full halogen chemistry scheme and grid-stretching capability.

Additionally, we improve the tropospheric AMF calculation with TROPOMI directionally DLER surface albedo data accounting for the geometrical dependency.

Our tropospheric BrO retrievals separate the tropospheric and stratospheric contributions from the total BrO columns and identify seasonal and latitudinal dependencies of tropospheric BrO columns. We find low tropospheric BrO columns of ~2.2×10^{13} molecules cm^{-2} at middle and low latitudes, possibly from SSA debromination and organobromine oxidation. Elevated tropospheric BrO columns up to 7.8×10^{13} molecules cm^{-2} are found over sea ice during the polar spring.

The retrieved TROPOMI tropospheric BrO columns align with the current GOME-2B product regarding the global distribution. Land-ocean contrast of tropospheric BrO columns over the tropical Pacific Ocean is similarly captured by TROPOMI satellite product and TORERO aircraft measurements ($r = 0.46$) with a discrepancy of less than 1.5×10^{13} molecules cm^{-2}. Compared with ground-based zenith-sky DOAS observations, we obtain a good consistency with a correlation coefficient of 0.67 and an average difference of 1.9×10^{13} molecules cm^{-2} for tropospheric BrO.

With a high spatial resolution of up to 5.5×3.5 km^2 and improved signal-to-noise, our TROPOMI product provides a unique opportunity to investigate the small-scale BrO enhancements from local sources, such as volcanic eruptions (e.g., at Raikoke, up to 8.0×10^{13} molecules cm^{-2}) and salt marsh (e.g., at the Rann of Kutch, up to 1.1×10^{14} molecules cm^{-2}). Comparing the TROPOMI product with model results provides indirect independent constraints on the Arctic bromine chemistry, acknowledging the uncertainties in satellite retrievals and halogen simulations. Model estimates of tropospheric BrO columns are generally improved by assuming a reduced salinity (0.01 practical salinity units), despite few discrepancies around Hudson Bay and Baffin Bay. Our TROPOMI BrO product provides high-resolution information for further studies of tropospheric BrO explosion events monitoring (Peng et al., 2021; Womack et al., 2023; Xia et al., 2022) and studies of bromine simulations in the troposphere.

In the future, our understanding of tropospheric bromine chemistry would be boosted by investigating the impact of critical parameters, such as snowpack salinity, snowpack and aerosol acidity, factors regulating direct bromine emissions from ozone oxidation ($O_3 + Br^-$), and initial conditions. More extended periods of ground-based BrO and aerosol bromide measurements, particularly close to local sources, are essential for evaluating bromine chemical mechanisms and validating satellite retrievals, alongside short-term field campaigns measuring vertical distributions of relevant gas and aerosol phase species. There are remaining gaps in our understanding of tropospheric bromine chemistry which would benefit from further studies, including data assimilation of multiple sources of observations and observational constraints on critical chemical parameters, both with modeling efforts.

Data Availability Statement

The monthly tropospheric BrO column product for 2019, Level-2 tropospheric BrO retrieval examples for springtime 2019, and configuration files of GEOS-Chem for this study are available on Harvard Dataverse (Y. Chen et al., 2023). Level-2 tropospheric BrO retrievals and codes are available upon request. Operational TROPOMI data are accessible via the Copernicus Open Access Hub for ozone (Copernicus Sentinel-5P, 2018a), NO_2 (Copernicus Sentinel-5P, 2018b), SO_2 (Copernicus Sentinel-5P, 2018c), and cloud (Copernicus Sentinel-5P, 2018d).

Acknowledgments

This work is funded by the National Natural Science Foundation of China (42375090, 42205134), the Shenzhen Key Laboratory of Precision Measurement and Early Warning Technology for Urban Environmental Health Risks (ZDSYS20220606100604008), Guangdong Basic and Applied Basic Research Fund (2020B1515130003), Guangdong Basic and Applied Basic Research Foundation (2021A1515110713), Guangdong University Research Project Science Team (2021KCXTD004), Major Talent Project of Guangdong Province (2021QN020924), and Shenzhen Science and Technology Program (KQTD20210811090048025, JCYJ20210324104604012, JCYJ20220530115404009). SS and AR gratefully acknowledge the funding by the Deutsche Forschungsgemeinschaft (DFG, German Research Foundation) - Projektnummer 268020496 – TRR 172, within the Transregional Collaborative Research Center "ArctiC Amplification: Climate Relevant Atmospheric and SurfaCe Processes, and Feedback Mechanisms (AC)³." XW was supported by the National Natural Science Foundation of China (42005083). RV acknowledges funding from the US National Science Foundation awards AGS-1104104 (TORERO project), and AGS-1951514. The involvement of the NSF-sponsored Lower Atmospheric Observing Facilities, managed and operated by the National Center for Atmospheric Research (NCAR) Earth Observing Laboratory (EOL), is acknowledged. The data was downloaded from the TORERO Data Archive, which is maintained by NCAR EOL. We acknowledge the free use of the TROPOMI surface DLER database provided through the Sentinel-5p+ Innovation project of ESA. The TROPOMI surface DLER database was created by the KNMI. We acknowledge EU/ESA/DLR for providing the TROPOMI level-2 data product of ozone, NO_2, SO_2, and cloud. This work is supported by the Center for Computational Science and Engineering at Southern University of Science and Technology.

References

Abbatt, J. P. D., Thomas, J. L., Abrahamsson, K., Boxe, C., Granfors, A., Jones, A. E., et al. (2012). Halogen activation via interactions with environmental ice and snow in the polar lower troposphere and other regions. *Atmospheric Chemistry and Physics*, *12*(14), 6237–6271. https://doi.org/10.5194/acp-12-6237-2012

Abrahamsson, K., Lorén, A., Wulff, A., & Wängberg, S. Å. (2004). Air–sea exchange of halocarbons: The influence of diurnal and regional variations and distribution of pigments. *Deep Sea Research Part II: Topical Studies in Oceanography*, *51*(22–24), 2789–2805. https://doi.org/10.1016/j.dsr2.2004.09.005

Afe, O. T., Richter, A., Sierk, B., Wittrock, F., & Burrows, J. P. (2004). BrO emission from volcanoes: A survey using GOME and SCIAMACHY measurements. *Geophysical Research Letters*, *31*(24), L24113. https://doi.org/10.1029/2004GL020994

Artiglia, L., Edebeli, J., Orlando, F., Chen, S., Lee, M. T., Corral Arroyo, P., et al. (2017). A surface-stabilized ozonide triggers bromide oxidation at the aqueous solution-vapour interface. *Nature Communications*, *8*(1), 700. https://doi.org/10.1038/s41467-017-00823-x

Avallone, L. M., Toohey, D. W., Fortin, T. J., McKinney, K. A., & Fuentes, J. D. (2003). In situ measurements of bromine oxide at two high-latitude boundary layer sites: Implications of variability. *Journal of Geophysical Research*, *108*(D3), 4089. https://doi.org/10.1029/2002JD002843

Badia, A., Reeves, C. E., Baker, A. R., Saiz-Lopez, A., Volkamer, R., Koenig, T. K., et al. (2019). Importance of reactive halogens in the tropical marine atmosphere: A regional modelling study using WRF-Chem. *Atmospheric Chemistry and Physics*, *19*(5), 3161–3189. https://doi.org/10.5194/acp-19-3161-2019

Barrie, L., & Platt, U. (1997). Arctic tropospheric chemistry: An overview. *Tellus B: Chemical and Physical Meteorology*, *49*(5), 450–454. https://doi.org/10.3402/tellusb.v49i5.15984

Begoin, M., Richter, A., Weber, M., Kaleschke, L., Tian-Kunze, X., Stohl, A., et al. (2010). Satellite observations of long range transport of a large BrO plume in the Arctic. *Atmospheric Chemistry and Physics*, *10*(14), 6515–6526. https://doi.org/10.5194/acp-10-6515-2010

Bey, I., Jacob, D. J., Yantosca, R. M., Logan, J. A., Field, B. D., Fiore, A. M., et al. (2001). Global modeling of tropospheric chemistry with assimilated meteorology: Model description and evaluation. *Journal of Geophysical Research*, *106*(D19), 23073–23095. https://doi.org/10.1029/2001JD000807

Bindle, L., Martin, R. V., Cooper, M. J., Lundgren, E. W., Eastham, S. D., Auer, B. M., et al. (2021). Grid-stretching capability for the GEOS-Chem 13.0. 0 atmospheric chemistry model. *Geoscientific Model Development*, *14*(10), 5977–5997. https://doi.org/10.5194/gmd-14-5977-2021

Blechschmidt, A.-M., Richter, A., Burrows, J., Kaleschke, L., Strong, K., Theys, N., et al. (2016). An exemplary case of a bromine explosion event linked to cyclone development in the Arctic. *Atmospheric Chemistry and Physics*, *16*(3), 1773–1788. https://doi.org/10.5194/acp-16-1773-2016

Bobrowski, N., Hönninger, G., Galle, B., & Platt, U. (2003). Detection of bromine monoxide in a volcanic plume. *Nature*, *423*(6937), 273–276. https://doi.org/10.1038/nature01625

Boersma, K. F., Eskes, H. J., & Brinksma, E. J. (2004). Error analysis for tropospheric NO_2 retrieval from space. *Journal of Geophysical Research*, *109*(D4), D04311. https://doi.org/10.1029/2003JD003962

Bougoudis, I., Blechschmidt, A.-M., Richter, A., Seo, S., Burrows, J. P., Theys, N., & Rinke, A. (2020). Long-term time series of Arctic tropospheric BrO derived from UV–VIS satellite remote sensing and its relation to first-year sea ice. *Atmospheric Chemistry and Physics*, *20*, 11869–11892. https://doi.org/10.5194/acp-20-11869-2020

Bovensmann, H., Burrows, J., Buchwitz, M., Frerick, J., Noël, S., Rozanov, V., et al. (1999). SCIAMACHY: Mission objectives and measurement modes. *Journal of the Atmospheric Sciences*, *56*(2), 127–150. https://doi.org/10.1175/1520-0469(1999)056<0127:SMOAMM>2.0.CO;2

Burrows, J. P., Weber, M., Buchwitz, M., Rozanov, V., Ladstätter-Weißenmayer, A., Richter, A., et al. (1999). The global ozone monitoring experiment (GOME): Mission concept and first scientific results. *Journal of the Atmospheric Sciences*, *56*(2), 151–175. https://doi.org/10.1175/1520-0469(1999)056<0151:TGOMEG>2.0.CO;2

Callies, J., Corpaccioli, E., Eisinger, M., Hahne, A., & Lefebvre, A. (2000). GOME-2-Metop's second-generation sensor for operational ozone monitoring. *ESA Bulletin*, *102*, 28–36.

Chance, K. (2006). Spectroscopic measurements of tropospheric composition from satellite measurements in the ultraviolet and visible: Steps toward continuous pollution monitoring from space. In *Remote sensing of the atmosphere for environmental security* (pp. 1–25). https://doi.org/10.1007/978-1-4020-5090-91

Chen, Q., Sherwen, T., Evans, M., & Alexander, B. (2018). DMS oxidation and sulfur aerosol formation in the marine troposphere: A focus on reactive halogen and multiphase chemistry. *Atmospheric Chemistry and Physics*, *18*, 13617–13637. https://doi.org/10.5194/acp-18-13617-2018

Chen, Y., Liu, S., Zhu, L., Seo, S., Richter, A., Li, X., et al. (2023). Global Observations of Tropospheric Bromine Monoxide (BrO) Columns from TROPOMI [Dataset]. Harvard Dataverse. https://doi.org/10.7910/DVN/REQ8GW

Choi, S., Theys, N., Salawitch, R., Wales, P., Joiner, J., Canty, T., et al. (2018). Link between Arctic tropospheric BrO explosion observed from space and sea-salt aerosols from blowing snow investigated using ozone monitoring instrument BrO data and GEOS-5 data assimilation system. *Journal of Geophysical Research: Atmospheres*, *123*(13), 6954–6983. https://doi.org/10.1029/2017JD026889

Choi, S., Wang, Y., Salawitch, R., Canty, T., Joiner, J., Zeng, T., et al. (2012). Analysis of satellite-derived Arctic tropospheric BrO columns in conjunction with aircraft measurements during ARCTAS and ARCPAC. *Atmospheric Chemistry and Physics*, *12*(3), 1255–1285. https://doi.org/10.5194/acp-12-1255-2012

Copernicus Sentinel-5P (processed by ESA). (2018a). TROPOMI Level 2 ozone total column products Version 01 [Dataset]. European Space Agency. https://doi.org/10.5270/S5P-fqouvyz

Copernicus Sentinel-5P (processed by ESA). (2018b). TROPOMI Level 2 nitrogen dioxide total column products Version 01 [Dataset]. European Space Agency. https://doi.org/10.5270/S5P-s4ljg54

Copernicus Sentinel-5P (processed by ESA). (2018c). TROPOMI Level 2 sulphur dioxide total column Version 01 [Dataset]. European Space Agency. https://doi.org/10.5270/S5P-yr8kdpp

Copernicus Sentinel-5P (processed by ESA). (2018d). TROPOMI Level 2 cloud products Version 01 [Dataset]. European Space Agency. https://doi.org/10.5270/S5P-ry8kaa5

Custard, K., Raso, A., Shepson, P., Staebler, R., & Pratt, K. (2017). Production and release of molecular bromine and chlorine from the Arctic coastal snowpack. *ACS Earth and Space Chemistry*, *1*(3), 142–151. https://doi.org/10.1021/acsearthspacechem.7b00014

De Smedt, I., Müller, J. F., Stavrakou, T., Van Der A, R., Eskes, H., & Van Roozendael, M. (2008). Twelve years of global observations of formaldehyde in the troposphere using GOME and SCIAMACHY sensors. *Atmospheric Chemistry and Physics*, *8*(16), 4947–4963. https://doi.org/10.5194/acp-8-4947-2008

De Smedt, I., Theys, N., Yu, H., Danckaert, T., Lerot, C., Compernolle, S., et al. (2018). Algorithm theoretical baseline for formaldehyde retrievals from S5P TROPOMI and from the QA4ECV project. *Atmospheric Measurement Techniques*, *11*(4), 2395–2426. https://doi.org/10.5194/amt-11-2395-2018

Dix, B., Koenig, T. K., & Volkamer, R. (2016). Parameterization retrieval of trace gas volume mixing ratios from Airborne MAX-DOAS. *Atmospheric Measurement Techniques*, *9*(11), 5655–5675. https://doi.org/10.5194/amt-9-5655-2016

Domine, F., Sparapani, R., Ianniello, A., & Beine, H. (2004). The origin of sea salt in snow on Arctic sea ice and in coastal regions. *Atmospheric Chemistry and Physics*, *4*(9/10), 2259–2271. https://doi.org/10.5194/acp-4-2259-2004

Eastham, S. D., Long, M. S., Keller, C. A., Lundgren, E., Yantosca, R. M., Zhuang, J., et al. (2018). GEOS-Chem High Performance (GCHP v11-02c): A next-generation implementation of the GEOS-Chem chemical transport model for massively parallel applications. *Geoscientific Model Development*, *11*(7), 2941–2953. https://doi.org/10.5194/gmd-11-2941-2018

Eastham, S. D., Weisenstein, D. K., & Barrett, S. R. (2014). Development and evaluation of the unified tropospheric–stratospheric chemistry extension (UCX) for the global chemistry-transport model GEOS-Chem. *Atmospheric Environment*, *89*, 52–63. https://doi.org/10.1016/j.atmosenv.2014.02.001

Falk, S., & Sinnhuber, B.-M. (2018). Polar boundary layer bromine explosion and ozone depletion events in the chemistry– climate model EMAC v2.52: Implementation and evaluation of AirSnow algorithm. *Geoscientific Model Development*, *11*(3), 1115–1131. https://doi.org/10.5194/gmd-11-1115-2018

Fan, S. M., & Jacob, D. J. (1992). Surface ozone depletion in the Arctic spring sustained by bromine reactions on aerosols. *Nature*, *359*(6395), 522–524. https://doi.org/10.1038/359522a0

Finlayson-Pitts, B. J. (2003). The tropospheric chemistry of sea salt: A molecular-level view of the chemistry of NaCl and NaBr. *Chemical Reviews*, *103*(12), 4801–4822. https://doi.org/10.1021/cr020653t

Fitzenberger, R., Bösch, H., Camy-Peyret, C., Chipperfield, M., Harder, H., Platt, U., et al. (2000). First profile measurements of tropospheric BrO. *Geophysical Research Letters*, *27*(18), 2921–2924. https://doi.org/10.1029/2000GL011531

Frey, M. M., Norris, S. J., Brooks, I. M., Anderson, P. S., Nishimura, K., Yang, X., et al. (2020). First direct observation of sea salt aerosol production from blowing snow above sea ice. *Atmospheric Chemistry and Physics*, *20*(4), 2549–2578. https://doi.org/10.5194/acp-20-2549-2020

Frinak, E. K., & Abbatt, J. P. D. (2006). Br2 production from the heterogeneous reaction of gas-phase OH with aqueous salt solutions: Impacts of acidity, halide concentration, and organic surfactants. *Journal of Physical Chemistry A*, *110*(35), 10456–10464. https://doi.org/10.1021/jp063165o

Garane, K., Koukouli, M.-E., Verhoelst, T., Lerot, C., Heue, K.-P., Fioletov, V., et al. (2019). TROPOMI/S5P total ozone column data: Global ground-based validation and consistency with other satellite missions. *Atmospheric Measurement Techniques*, *12*(10), 5263–5287. https://doi.org/10.5194/amt-12-5263-2019

Gelaro, R., McCarty, W., Suárez, M. J., Todling, R., Molod, A., Takacs, L., et al. (2017). The Modern-Era Retrospective Analysis for Research and Applications, version 2 (MERRA-2). *Journal of Climate*, *30*(14), 5419–5454. https://doi.org/10.1175/JCLI-D-16-0758.1

Gilman, J. B., Burkhart, J. F., Lerner, B. M., Williams, E. J., Kuster, W., Goldan, P. D., et al. (2010). Ozone variability and halogen oxidation within the Arctic and sub-Arctic springtime boundary layer. *Atmospheric Chemistry and Physics*, *10*(21), 10223–10236. https://doi.org/10.5194/acp-10-10223-2010

Guenther, A. B., Jiang, X., Heald, C. L., Sakulyanontvittaya, T., Duhl, T., Emmons, L. K., & Wang, X. (2012). The Model of Emissions of Gases and Aerosols from Nature version 2.1 (MEGAN2.1): An extended and updated framework for modeling biogenic emissions. *Geoscientific Model Development*, *5*(6), 1471–1492. https://doi.org/10.5194/gmd-5-1471-2012

Guenther, A. B., Jiang, X., Shah, T., Huang, L., Kemball-Cook, S., & Yarwood, G. (2019). Model of emissions of gases and aerosol from nature version 3 (MEGAN3). In *Air pollution modeling and its application XXVI 36* (pp. 187–192). Springer International Publishing. https://doi.org/10.1007/978-3-030-22055-6_29

Gutmann, A., Bobrowski, N., Roberts, T. J., Rüdiger, J., & Hoffmann, T. (2018). Advances in bromine speciation in volcanic plumes. *Frontiers in Earth Science*, *6*, 213. https://doi.org/10.3389/feart.2018.00213

Halfacre, J., Shepson, P. B., & Pratt, K. A. (2019). pH-dependent production of molecular chlorine, bromine, and iodine from frozen saline surfaces. *Atmospheric Chemistry and Physics*, *19*(7), 4917–4931. https://doi.org/10.5194/acp-19-4917-2019

Hausmann, M., & Platt, U. (1994). Spectroscopic measurement of bromine oxide and ozone in the high Arctic during Polar Sunrise Experiment 1992. *Journal of Geophysical Research*, *99*(D12), 25399–25413. https://doi.org/10.1029/94JD0131

Hebestreit, K., Stutz, J., Rosen, D., Matveiv, V., Peleg, M., Luria, M., & Platt, U. (1999). DOAS measurements of tropospheric bromine oxide in mid-latitudes. *Science*, *283*(5398), 55–57. https://doi.org/10.1126/science.283.5398.55

Hedelt, P., Efremenko, D. S., Loyola, D. G., Spurr, R., & Clarisse, L. (2019). Sulfur dioxide layer height retrieval from Sentinel-5 Precursor/TROPOMI using FP_ILM. *Atmospheric Measurement Techniques*, *12*(10), 5503–5517. https://doi.org/10.5194/amt-12-5503-2019

Hendrick, F., van Roozendael, M., Chipperfield, M. P., Dorf, M., Goutail, F., Yang, X., et al. (2007). Retrieval of stratospheric and tropospheric BrO profiles and columns using ground-based zenith-sky DOAS observations at Harestua, 60 N. *Atmospheric Chemistry and Physics*, *7*(18), 4869–4885. https://doi.org/10.5194/acp-7-4869-2007

Herrmann, M., Schöne, M., Borger, C., Warnach, S., Wagner, T., Platt, U., & Gutheil, E. (2022). Ozone depletion events in the Arctic spring of 2019: A new modeling approach to bromine emissions. *Atmospheric Chemistry and Physics*, *22*(20), 13495–13526. https://doi.org/10.5194/acp-22-13495-2022

Herrmann, M., Sihler, H., Frieß, U., Wagner, T., Platt, U., & Gutheil, E. (2021). Time-dependent 3D simulations of tropospheric ozone depletion events in the Arctic spring using the Weather Research and Forecasting model coupled with Chemistry (WRF-Chem). *Atmospheric Chemistry and Physics*, *21*(10), 7611–7638. https://doi.org/10.5194/acp-21-7611-2021

Heue, K.-P., Brenninkmeijer, C., Baker, A., Rauthe-Schöch, A., Walter, D., Wagner, T., et al. (2011). SO_2 and BrO observation in the plume of the Eyjafjallajökull volcano 2010: CARIBIC and GOME-2 retrievals. *Atmospheric Chemistry and Physics*, *11*(6), 2973–2989. https://doi.org/10.5194/acp-11-2973-2011

Heue, K.-P., Eichmann, K.-U., & Valks, P. (2021). ATBD for tropospheric ozone column. S5P-L2-DLR-ATBD-400C, V2.3, issue 2.3, June. Retrieved from https://sentinels.copernicus.eu/web/sentinel/technical-guides/sentinel-5p/products-algorithms

Heue, K.-P., Spurr, R., Loyola, D., Van Roozendael, M., Lerot, C., & Xu, J. (2021). ATBD for total ozone column. S5P-L2-DLR-ATBD-400A, V2.3, issue 2.1, June. Retrieved from https://sentinels.copernicus.eu/web/sentinel/technical-guides/sentinel-5p/products-algorithms

Hoesly, R. M., Smith, S. J., Feng, L., Klimont, Z., Janssens-Maenhout, G., Pitkanen, T., et al. (2018). Historical (1750–2014) anthropogenic emissions of reactive gases and aerosols from the Community Emissions Data System (CEDS). *Geoscientific Model Development*, *11*(1), 369–408. https://doi.org/10.5194/gmd-11-369-2018

Hollwedel, J., Wenig, M., Beirle, S., Kraus, S., Kühl, S., Wilms-Grabe, W., et al. (2004). Year-to-year variations of spring time polar tropospheric BrO as seen by GOME. *Advances in Space Research*, *34*(4), 804–808. https://doi.org/10.1016/j.asr.2003.08.060

Holmes, C. D., Jacob, D. J., Corbitt, E. S., Mao, J., Yang, X., Talbot, R., & Slemr, F. (2010). Global atmospheric model for mercury including oxidation by bromine atoms. *Atmospheric Chemistry and Physics*, *10*(24), 12037–12057. https://doi.org/10.5194/acp-10-12037-2010

Holmes, C. D., Jacob, D. J., & Yang, X. (2006). Global lifetime of elemental mercury against oxidation by atomic bromine in the free troposphere. *Geophysical Research Letters*, *33*(20), L20808. https://doi.org/10.1029/2006GL027176

Hönninger, G., Bobrowski, N., Palenque, E., Torrez, R., & Platt, U. (2004). Reactive bromine and sulfur emissions at Salar de Uyuni, Bolivia. *Geophysical Research Letters*, *31*(4), L04101. https://doi.org/10.1029/2003GL018818

Hörmann, C., Sihler, H., Beirle, S., Penning de Vries, M., Platt, U., & Wagner, T. (2016). Seasonal variation of tropospheric bromine monoxide over the Rann of Kutch salt marsh seen from space. *Atmospheric Chemistry and Physics*, *16*(20), 13015–13034. https://doi.org/10.5194/acp-16-13015-2016

Huang, J., & Jaeglé, L. (2017). Wintertime enhancements of sea salt aerosol in polar regions consistent with a sea ice source from blowing snow. *Atmospheric Chemistry and Physics*, *17*(5), 3699–3712. https://doi.org/10.5194/acp-17-3699-2017

Huang, J., Jaeglé, L., Chen, Q., Alexander, B., Sherwen, T., Evans, M. J., et al. (2020). Evaluating the impact of blowing-snow sea salt aerosol on springtime BrO and O_3 in the Arctic. *Atmospheric Chemistry and Physics*, *20*(12), 7335–7358. https://doi.org/10.5194/acp-20-7335-2020

Huang, J., Jaeglé, L., & Shah, V. (2018). Using CALIOP to constrain blowing snow emissions of sea salt aerosols over Arctic and Antarctic sea ice. *Atmospheric Chemistry and Physics*, *18*(22), 16253–16269. https://doi.org/10.5194/acp-18-16253-2018

Ioannidis, E., Law, K., Raut, J. C., Marelle, L., Onishi, T., Kirpes, R. M., et al. (2023). Modelling wintertime sea-spray aerosols under Arctic haze conditions. *Atmospheric Chemistry and Physics*, *23*(10), 5641–5678. https://doi.org/10.5194/acp-23-5641-2023

Jeong, D., McNamara, S. M., Barget, A. J., Raso, A. R., Upchurch, L. M., Thanekar, S., et al. (2022). Multiphase reactive bromine chemistry during late spring in the Arctic: Measurements of gases, particles, and snow. *ACS Earth and Space Chemistry*, *6*(12), 2877–2887. https://doi.org/10.1021/acsearthspacechem.2c00189

Kaiser, J., Heil, A., Andreae, M., Benedetti, A., Chubarova, N., Jones, L., et al. (2012). Biomass burning emissions estimated with a global fire assimilation system based on observed fire radiative power. *Biogeosciences*, *9*(1), 527–554. https://doi.org/10.5194/bg-9-527-2012

Kerkweg, A., Jöckel, P., Warwick, N., Gebhardt, S., Brenninkmeijer, C., & Lelieveld, J. (2008). Consistent simulation of bromine chemistry from the marine boundary layer to the stratosphere–Part 2: Bromocarbons. *Atmospheric Chemistry and Physics*, *8*(19), 5919–5939. https://doi.org/10.5194/acp-8-5919-2008

Kleipool, Q. L., Dobber, M. R., de Haan, J., & Levelt, P. F. (2008). Earth surface reflectance climatology from 3 years of OMI data. *Journal of Geophysical Research*, *113*(D18), D18308. https://doi.org/10.1029/2008JD010290

Koenig, T. K., Volkamer, R., Baidar, S., Dix, B., Wang, S., Anderson, D. C., et al. (2017). BrO and inferred Br y profiles over the western Pacific: Relevance of inorganic bromine sources and a Br_y minimum in the aged tropical tropopause layer. *Atmospheric Chemistry and Physics*, *17*(24), 15245–15270. https://doi.org/10.5194/acp-17-15245-2017

Krnavek, L., Simpson, W. R., Carlson, D., Domine, F., Douglas, T. A., & Sturm, M. (2012). The chemical composition of surface snow in the Arctic: Examining marine, terrestrial, and atmospheric influences. *Atmospheric Environment*, *50*, 349–359. https://doi.org/10.1016/j.atmosenv.2011.11.033

Latsch, M., Richter, A., Eskes, H., Sneep, M., Wang, P., Veefkind, P., et al. (2022). Intercomparison of Sentinel-5P TROPOMI cloud products for tropospheric trace gas retrievals. *Atmospheric Measurement Techniques*, *15*(21), 6257–6283. https://doi.org/10.5194/amt-15-6257-2022

Le Breton, M., Bannan, T. J., Shallcross, D. E., Khan, M. A., Evans, M. J., Lee, J., et al. (2017). Enhanced ozone loss by active inorganic bromine chemistry in the tropical troposphere. *Atmospheric Environment*, *155*, 21–28. https://doi.org/10.1016/j.atmosenv.2017.02.003

Levelt, P. F., Joiner, J., Tamminen, J., Veefkind, J. P., Bhartia, P. K., Stein Zweers, D. C., et al. (2018). The Ozone Monitoring Instrument: Overview of 14 years in space. *Atmospheric Chemistry and Physics*, *18*(8), 5699–5745. https://doi.org/10.5194/acp-18-5699-2018

Levelt, P. F., van den Oord, G. H., Dobber, M. R., Malkki, A., Visser, H., De Vries, J., et al. (2006). The ozone monitoring instrument. *IEEE Transactions on Geoscience and Remote Sensing*, *44*(5), 1093–1101. https://doi.org/10.1109/TGRS.2006.872333

Liao, J., Huey, L., Tanner, D., Flocke, F., Orlando, J., Neuman, J., et al. (2012). Observations of inorganic bromine (HOBr, BrO, and Br_2) speciation at Barrow, Alaska, in spring 2009. *Journal of Geophysical Research*, *117*(D14), D00R16. https://doi.org/10.1029/2011JD016641

Liao, J., Sihler, H., Huey, L., Neuman, J., Tanner, D., Friess, U., et al. (2011). A comparison of Arctic BrO measurements by chemical ionization mass spectrometry and long path-differential optical absorption spectroscopy. *Journal of Geophysical Research*, *116*, D00R02. https://doi.org/10.1029/2010JD014788

Liu, S., Valks, P., Pinardi, G., De Smedt, I., Yu, H., Beirle, S., & Richter, A. (2019). An improved total and tropospheric NO_2 column retrieval for GOME-2. *Atmospheric Measurement Techniques*, *12*(2), 1029–1057. https://doi.org/10.5194/amt-12-1029-2019

Liu, S., Valks, P., Pinardi, G., Xu, J., Argyrouli, A., Lutz, R., et al. (2020). An improved air mass factor calculation for nitrogen dioxide measurements from the Global Ozone Monitoring Experiment-2 (GOME-2). *Atmospheric Measurement Techniques*, *13*(2), 755–787. https://doi.org/10.5194/amt-13-755-2020

Liu, S., Valks, P., Pinardi, G., Xu, J., Chan, K. L., Argyrouli, A., et al. (2021). An improved TROPOMI tropospheric NO_2 research product over Europe. *Atmospheric Measurement Techniques*, *14*(11), 7297–7327. https://doi.org/10.5194/amt-14-7297-2021

Long, M., Keene, W., Easter, R. C., Sander, R., Liu, X., Kerkweg, A., & Erickson, D. (2014). Sensitivity of tropospheric chemical composition to halogen-radical chemistry using a fully coupled size-resolved multiphase chemistry–global climate system: Halogen distributions, aerosol composition, and sensitivity of climate-relevant gases. *Atmospheric Chemistry and Physics*, *14*(7), 3397–3425. https://doi.org/10.5194/acp-14-3397-2014

Loyola, D. G., Lutz, R., Argyrouli, A., & Spurr, R. (2020). S5P/TROPOMI ATBD cloud products. Tech. rep., S5P-DLR-L2-ATBD-400I issue 2.2.

Loyola, D. G., Gimeno García, S., Lutz, R., Argyrouli, A., Romahn, F., Spurr, R. J., et al. (2018). The operational cloud retrieval algorithms from TROPOMI on board Sentinel-5 Precursor. *Atmospheric Measurement Techniques*, *11*(1), 409–427. https://doi.org/10.5194/amt-11-409-2018

Lutz, R., Loyola, D., Gimeno García, S., & Romahn, F. (2016). OCRA radiometric cloud fractions for GOME-2 on MetOp-A/B. *Atmospheric Measurement Techniques*, *9*(5), 2357–2379. https://doi.org/10.5194/amt-9-2357-2016

Marelle, L., Thomas, J. L., Ahmed, S., Tuite, K., Stutz, J., Dommergue, A., et al. (2021). Implementation and impacts of surface and blowing snow sources of Arctic bromine activation within WRF-Chem 4.1. 1. *Journal of Advances in Modeling Earth Systems*, *13*(8), e2020MS002391. https://doi.org/10.1029/2020MS002391

Martin, R. S., Roberts, T. J., Mather, T. A., & Pyle, D. M. (2009). The implications of H2S and H2 kinetic stability in high-T mixtures of magmatic and atmospheric gases for the production of oxidized trace species (eg, BrO and NOx). *Chemical Geology*, *263*(1–4), 143–150. https://doi.org/10.1016/j.chemgeo.2008.12.028

Martin, R. V., Chance, K., Jacob, D. J., Kurosu, T. P., Spurr, R. J., Bucsela, E., et al. (2002). An improved retrieval of tropospheric nitrogen dioxide from GOME. *Journal of Geophysical Research*, *107*(D20), ACH9-1–ACH9-21. https://doi.org/10.1029/2001JD001027

Matveev, V., Peleg, M., Rosen, D., Tov-Alper, D. S., Hebestreit, K., Stutz, J., et al. (2001). Bromine oxide—Ozone interaction over the Dead Sea. *Journal of Geophysical Research*, *106*(D10), 10375–10387. https://doi.org/10.1029/2000JD900611

McGonigle, A., Delmelle, P., Oppenheimer, C., Tsanev, V., Delfosse, T., Williams-Jones, G., et al. (2004). SO_2 depletion in tropospheric volcanic plumes. *Geophysical Research Letters*, *31*(13), L13201. https://doi.org/10.1029/2004GL019990

McMullan, K., & van der Meulen, W. (2013). SENTINEL-5 precursor system. In *ESA living planet symposium, 9–13 September 2013, Edinburgh, UK* (p. 140).

Munro, R., Lang, R., Klaes, D., Poli, G., Retscher, C., Lindstrot, R., et al. (2016). The GOME-2 instrument on the Metop series of satellites: Instrument design, calibration, and level 1 data processing – An overview. *Atmospheric Measurement Techniques*, *9*(3), 1279–1301. https://doi.org/10.5194/amt-9-1279-2016

Neuman, J. A., Nowak, J. B., Huey, L. G., Burkholder, J. B., Dibb, J. E., Holloway, J. S., et al. (2010). Bromine measurements in ozone depleted air over the Arctic Ocean. *Atmospheric Chemistry and Physics*, *10*(14), 6503–6514. https://doi.org/10.5194/acp-10-6503-2010

Newberg, J. T., Matthew, B. M., & Anastasio, C. (2005). Chloride and bromide depletions in sea-salt particles over the northeastern Pacific Ocean. *Journal of Geophysical Research*, *110*(D6), D06209. https://doi.org/10.1029/2004JD005446

Ninomiya, Y., Hashimoto, S., Kawasaki, M., & Wallington, T. J. (2000). Cavity ring-down study of BrO radicals: Kinetics of the $Br^+ O_3$ reaction and rate of relaxation of vibrationally excited BrO by collisions with N2 and O2. *International Journal of Chemical Kinetics*, *32*(3), 125–130. https://doi.org/10.1002/(SICI)1097-4601(2000)32:3<125::AID-KIN1>3.0.CO;2-4

Nomura, D., Granskog, M. A., Fransson, A., Chierici, M., Silyakova, A., Ohshima, K. I., et al. (2018). CO_2 flux over young and snow-covered Arctic pack ice in winter and spring. *Biogeosciences*, *15*(11), 3331–3343. https://doi.org/10.5194/bg-15-3331-2018

Oppenheimer, C., Tsanev, V. I., Braban, C. F., Cox, R. A., Adams, J. W., Aiuppa, A., et al. (2006). BrO formation in volcanic plumes. *Geochimica et Cosmochimica Acta*, *70*(12), 2935–2941. https://doi.org/10.1016/j.gca.2006.04.001

Ordóñez, C., Lamarque, J.-F., Tilmes, S., Kinnison, D. E., Atlas, E. L., Blake, D. R., et al. (2012). Bromine and iodine chemistry in a global chemistry-climate model: Description and evaluation of very short-lived oceanic sources. *Atmospheric Chemistry and Physics*, *12*(3), 1423–1447. https://doi.org/10.5194/acp-12-1423-2012

Palmer, P. I., Jacob, D. J., Chance, K., Martin, R. V., Spurr, R. J., Kurosu, T. P., et al. (2001). Air mass factor formulation for spectroscopic measurements from satellites: Application to formaldehyde retrievals from the Global Ozone Monitoring Experiment. *Journal of Geophysical Research*, *106*(D13), 14539–14550. https://doi.org/10.1029/2000JD900772

Parrella, J., Jacob, D. J., Liang, Q., Zhang, Y., Mickley, L. J., Miller, B., et al. (2012). Tropospheric bromine chemistry: Implications for present and pre-industrial ozone and mercury. *Atmospheric Chemistry and Physics*, *12*(15), 6723–6740. https://doi.org/10.5194/acp-12-6723-2012

Peng, X., Wang, W., Xia, M., Chen, H., Ravishankara, A. R., Li, Q., et al. (2021). An unexpected large continental source of reactive bromine and chlorine with significant impact on wintertime air quality. *National Science Review*, *8*(7), nwaa304. https://doi.org/10.1093/nsr/nwaa304

Peterson, P. K., Hartwig, M., May, N. W., Schwartz, E., Rigor, I., Ermold, W., et al. (2019). Snowpack measurements suggest role for multi-year sea ice regions in Arctic atmospheric bromine and chlorine chemistry. *Elementa: Science of the Anthropocene*, *7*, 14. https://doi.org/10.1525/elementa.352

Peterson, P. K., Pöhler, D., Sihler, H., Zielcke, J., General, S., Frieß, U., et al. (2017). Observations of bromine monoxide transport in the Arctic sustained on aerosol particles. *Atmospheric Chemistry and Physics*, *17*(12), 7567–7579. https://doi.org/10.5194/acp-17-7567-2017

Peterson, P. K., Pöhler, D., Zielcke, J., General, S., Frieß, U., Platt, U., et al. (2018). Springtime bromine activation over coastal and inland Arctic snowpacks. *ACS Earth and Space Chemistry*, *2*(10), 1075–1086. https://doi.org/10.1021/acsearthspacechem.8b00083

Peterson, P. K., Pratt, K. A., Simpson, W. R., Nghiem, S. V., Pérez Pérez, L., Boone, E. J., et al. (2016). The role of open lead interactions in atmospheric ozone variability between Arctic coastal and inland sites. *Elementa: Science of the Anthropocene*, *4*, 000109. https://doi.org/10.12952/journal.elementa.000109

Peterson, P. K., Simpson, W. R., & Nghiem, S. V. (2016). Variability of bromine monoxide at Barrow, Alaska, over four halogen activation (March–May) seasons and at two on-ice locations. *Journal of Geophysical Research: Atmospheres*, *121*(3), 1381–1396. https://doi.org/10.1002/2015JD024094

Peterson, P. K., Simpson, W. R., Pratt, K. A., Shepson, P. B., Frieß, U., Zielcke, J., et al. (2015). Dependence of the vertical distribution of bromine monoxide in the lower troposphere on meteorological factors such as wind speed and stability. *Atmospheric Chemistry and Physics*, *15*(4), 2119–2137. https://doi.org/10.5194/acp-15-2119-2015

Platt, U., & Stutz, J. (2008). *Differential absorption spectroscopy* (pp. 135–174). Springer Berlin Heidelberg. https://doi.org/10.1007/978-3-540-75776-4_6

Platt, U., & Wagner, T. (1998). Satellite mapping of enhanced BrO concentrations in the troposphere. *Nature*, *395*(6701), 486–490. https://doi.org/10.1038/26723

Prados-Roman, C., Gómez-Martín, L., Puentedura, O., Navarro-Comas, M., Iglesias, J., De Mingo, J. R., et al. (2018). Reactive bromine in the low troposphere of Antarctica: Estimations at two research sites. *Atmospheric Chemistry and Physics*, *18*(12), 8549–8570. https://doi.org/10.5194/acp-18-8549-2018

Pratt, K. A., Custard, K. D., Shepson, P. B., Douglas, T. A., P¨ohler, D., General, S., et al. (2013). Photochemical production of molecular bromine in Arctic surface snowpacks. *Nature Geoscience*, *6*(5), 351–356. https://doi.org/10.1038/ngeo1779

Read, K. A., Mahajan, A. S., Carpenter, L. J., Evans, M. J., Faria, B. V., Heard, D. E., et al. (2008). Extensive halogen-mediated ozone destruction over the tropical Atlantic Ocean. *Nature*, *453*(7199), 1232–1235. https://doi.org/10.1038/nature07035

Richter, A., Begoin, M., Hilboll, A., & Burrows, J. (2011). An improved NO_2 retrieval for the GOME-2 satellite instrument. *Atmospheric Measurement Techniques*, *4*(6), 1147–1159. https://doi.org/10.5194/amt-4-1147-2011

Richter, A., Wittrock, F., Eisinger, M., & Burrows, J. P. (1998). GOME observations of tropospheric BrO in northern hemispheric spring and summer 1997. *Geophysical Research Letters*, *25*(14), 2683–2686. https://doi.org/10.1029/98GL52016

Richter, A., Wittrock, F., Ladstätter-Weißenmayer, A., & Burrows, J. (2002). GOME measurements of stratospheric and tropospheric BrO. *Advances in Space Research*, *29*(11), 1667–1672. https://doi.org/10.1016/S0273-1177(02)00123-0

Roscoe, H., Brough, N., Jones, A., Wittrock, F., Richter, A., van Roozendael, M., & Hendrick, F. (2014). Characterisation of vertical BrO distribution during events of enhanced tropospheric BrO in Antarctica, from combined remote and in-situ measurements. *Journal of Quantitative Spectroscopy and Radiative Transfer*, *138*, 70–81. https://doi.org/10.1016/j.jqsrt.2014.01.026

Saiz-Lopez, A., Lamarque, J.-F., Kinnison, D. E., Tilmes, S., Ordóñez, C., Orlando, J. J., et al. (2012). Estimating the climate significance of halogen-driven ozone loss in the tropical marine troposphere. *Atmospheric Chemistry and Physics*, *12*(9), 3939–3949. https://doi.org/10.5194/acp-12-3939-2012

Saiz-Lopez, A., & von Glasow, R. (2012). Reactive halogen chemistry in the troposphere. *Chemical Society Reviews*, *41*(19), 6448–6472. https://doi.org/10.1039/c2cs35208g

Salawitch, R., Canty, T., Kurosu, T., Chance, K., Liang, Q., da Silva, A., et al. (2010). A new interpretation of total column BrO during Arctic spring. *Geophysical Research Letters*, *37*(21), L21805. https://doi.org/10.1029/2010GL043798

Sander, R., Burrows, J., & Kaleschke, L. (2006). Carbonate precipitation in brine–a potential trigger for tropospheric ozone depletion events. *Atmospheric Chemistry and Physics*, *6*(12), 4653–4658. https://doi.org/10.5194/acp-6-4653-2006

Sander, R., & Crutzen, P. J. (1996). Model study indicating halogen activation and ozone destruction in polluted air masses transported to the sea. *Journal of Geophysical Research*, *101*(D4), 9121–9138. https://doi.org/10.1029/95JD03793

Sander, R., Keene, W. C., Pszenny, A. A. P., Arimoto, R., Ayers, G. P., Baboukas, E., et al. (2003). Inorganic bromine in the marine boundary layer: A critical review. *Atmospheric Chemistry and Physics*, *3*(5), 1301–1336. https://doi.org/10.5194/acp-3-1301-2003

Schmidt, J. A., Jacob, D., Horowitz, H. M., Hu, L., Sherwen, T., Evans, M. J., et al. (2016). Modeling the observed tropospheric BrO background: Importance of multiphase chemistry and implications for ozone, OH, and mercury. *Journal of Geophysical Research: Atmospheres*, *121*(19), 11819–11835. https://doi.org/10.1002/2015JD024229

Seo, S., Richter, A., Blechschmidt, A.-M., Bougoudis, I., & Burrows, J. P. (2019). First high-resolution BrO column retrievals from TROPOMI. *Atmospheric Measurement Techniques*, *12*(5), 2913–2932. https://doi.org/10.5194/amt-12-2913-2019

Sherwen, T., Schmidt, J. A., Evans, M. J., Carpenter, L. J., Großmann, K., Eastham, S. D., et al. (2016). Global impacts of tropospheric halogens (Cl, Br, I) on oxidants and composition in GEOS-Chem. *Atmospheric Chemistry and Physics*, *16*(18), 12239–12271. https://doi.org/10.5194/acp-16-12239-2016

Sihler, H., Platt, U., Beirle, S., Marbach, T., Kühl, S., Dörner, S., et al. (2012). Tropospheric BrO column densities in the Arctic derived from satellite: Retrieval and comparison to ground-based measurements. *Atmospheric Measurement Techniques*, *5*(11), 2779–2807. https://doi.org/10.5194/amt-5-2779-2012

Simpson, W. R., Brown, S. S., Saiz-Lopez, A., Thornton, J. A., & von Glasow, R. (2015). Tropospheric halogen chemistry: Sources, cycling, and impacts. *Chemical Reviews*, *115*(10), 4035–4062. https://doi.org/10.1021/cr5006638

Simpson, W. R., Frieß, U., Thomas, J. L., Lampel, J., & Platt, U. (2018). Polar nighttime chemistry produces intense reactive bromine events. *Geophysical Research Letters*, *45*(18), 9987–9994. https://doi.org/10.1029/2018GL079444

Simpson, W. R., Peterson, P. K., Frieß, U., Sihler, H., Lampel, J., Platt, U., et al. (2017). Horizontal and vertical structure of reactive bromine events probed by bromine monoxide MAX-DOAS. *Atmospheric Chemistry and Physics*, *17*(15), 9291–9309. https://doi.org/10.5194/acp-17-9291-2017

Simpson, W. R., von Glasow, R., Riedel, K., Anderson, P., Ariya, P., Bottenheim, J., et al. (2007). Halogens and their role in polar boundary-layer ozone depletion. *Atmospheric Chemistry and Physics*, *7*(16), 4375–4418. https://doi.org/10.5194/acp-7-4375-2007

Sjostedt, S. J., & Abbatt, J. P. D. (2008). Release of gas-phase halogens from sodium halide substrates: Heterogeneous oxidation of frozen solutions and desiccated salts by hydroxyl radicals. *Environmental Research Letters*, *3*(4), 045007. https://doi.org/10.1088/1748-9326/3/4/045007

Spurr, R. J. (2006). VLIDORT: A linearized pseudo-spherical vector discrete ordinate radiative transfer code for forward model and retrieval studies in multilayer multiple scattering media. *Journal of Quantitative Spectroscopy and Radiative Transfer*, *102*(2), 316–342. https://doi.org/10.1016/j.jqsrt.2006.05.005

Steffen, W., Sanderson, R. A., Tyson, P. D., Jäger, J., Matson, P. A., Moore, B., III., et al. (2006). *Global change and the earth system: A planet under pressure*. Springer Science & Business Media. https://doi.org/10.1579/0044-7447(2007)36[614:TAAHNO]2.0.CO;2

Stutz, J., Ackermann, R., Fast, J. D., & Barrie, L. (2002). Atmospheric reactive chlorine and bromine at the Great Salt Lake, Utah. *Geophysical Research Letters*, *29*(10), 1811–1814. https://doi.org/10.1029/2002GL014812

Stutz, J., Thomas, J. L., Hurlock, S. C., Schneider, M., Von Glasow, R., Piot, M., et al. (2011). Longpath DOAS observations of surface BrO at Summit, Greenland. *Atmospheric Chemistry and Physics*, *11*(18), 9899–9910. https://doi.org/10.5194/acp-11-9899-2011

Suleiman, R. M., Chance, K., Liu, X., González Abad, G., Kurosu, T. P., Hendrick, F., & Theys, N. (2019). OMI total bromine monoxide (OMBRO) data product: Algorithm, retrieval and measurement comparisons. *Atmospheric Measurement Techniques*, *12*(4), 2067–2084. https://doi.org/10.5194/amt-12-2067-2019

Surl, L., Donohoue, D., Aiuppa, A., Bobrowski, N., & von Glasow, R. (2015). Quantification of the depletion of ozone in the plume of Mount Etna. *Atmospheric Chemistry and Physics*, *15*(5), 2613–2628. https://doi.org/10.5194/acp-15-2613-2015

Swanson, W. F., Holmes, C. D., Simpson, W. R., Confer, K., Marelle, L., Thomas, J. L., et al. (2022). Comparison of model and ground observations finds snowpack and blowing snow aerosols both contribute to Arctic tropospheric reactive bromine. *Atmospheric Chemistry and Physics*, *22*(22), 14467–14488. https://doi.org/10.5194/acp-22-14467-2022

Tas, E., Peleg, M., Matveev, V., Zingler, J., & Luria, M. (2005). Frequency and extent of bromine oxide formation over the Dead Sea. *Journal of Geophysical Research*, *110*(D11), D11304. https://doi.org/10.1029/2004JD005665

Theys, N., De Smedt, I., Yu, H., Danckaert, T., van Gent, J., Hörmann, C., et al. (2017). Sulfur dioxide retrievals from TROPOMI onboard Sentinel-5 Precursor: Algorithm theoretical basis. *Atmospheric Measurement Techniques*, *10*(1), 119–153. https://doi.org/10.5194/amt-10-119-2017

Theys, N., van Roozendael, M., Dils, B., Hendrick, F., Hao, N., & De Maziere, M. (2009). First satellite detection of volcanic bromine monoxide emission after the Kasatochi eruption. *Geophysical Research Letters*, *36*(3), L03809. https://doi.org/10.1029/2008GL036552

Theys, N., van Roozendael, M., Errera, Q., Hendrick, F., Daerden, F., Chabrillat, S., et al. (2009). A global stratospheric bromine monoxide climatology based on the BASCOE chemical transport model. *Atmospheric Chemistry and Physics*, *9*(3), 831–848. https://doi.org/10.5194/acp-9-831-2009

Theys, N., van Roozendael, M., Hendrick, F., Yang, X., Smedt, I. D., Richter, A., et al. (2011). Global observations of tropospheric BrO columns using GOME-2 satellite data. *Atmospheric Chemistry and Physics*, *11*(4), 1791–1811. https://doi.org/10.5194/acp-11-1791-2011

Tilstra, L. G., Tuinder, O., Wang, P., & Stammes, P. (2017). Surface reflectivity climatologies from UV to NIR determined from Earth observations by GOME-2 and SCIAMACHY. *Journal of Geophysical Research: Atmospheres*, *122*(7), 4084–4111. https://doi.org/10.1002/2016JD025940

Tilstra, L. G. (2022). TROPOMI ATBD of the directionally dependent surface Lambertian-equivalent reflectivity. KNMI Report S5P-KNMI-L3-0301-RP, Issue 1.2.0, January 13, 2022.

Tilstra, L. G., Tuinder, O. N., Wang, P., & Stammes, P. (2021). Directionally dependent Lambertian-equivalent reflectivity (DLER) of the Earth's surface measured by the GOME-2 satellite instruments. *Atmospheric Measurement Techniques*, *14*(6), 4219–4238. https://doi.org/10.5194/amt-14-4219-2021

Tonboe, R. T., Nandan, V., Mäkynen, M., Pedersen, L. T., Kern, S., Lavergne, T., et al. (2021). Simulated geophysical noise in sea ice concentration estimates of open water and snow-covered sea ice. *IEEE Journal of Selected Topics in Applied Earth Observations and Remote Sensing*, *15*, 1309–1326. https://doi.org/10.1109/JSTARS.2021.3134021

Toyota, K., McConnell, J. C., Lupu, A., Neary, L., McLinden, C. A., Richter, A., et al. (2011). Analysis of reactive bromine production and ozone depletion in the Arctic boundary layer using 3-D simulations with GEM-AQ: Inference from synoptic-scale patterns. *Atmospheric Chemistry and Physics*, *11*(8), 3949–3979. https://doi.org/10.5194/acp-11-3949-2011

van Geffen, J., Boersma, K. F., Eskes, H., Sneep, M., Ter Linden, M., Zara, M., & Veefkind, J. P. (2020). S5P TROPOMI NO_2 slant column retrieval: Method, stability, uncertainties and comparisons with OMI. *Atmospheric Measurement Techniques*, *13*(3), 1315–1335. https://doi.org/10.5194/amt-13-1315-2020

Veefkind, J., Aben, I., McMullan, K., Förster, H., De Vries, J., Otter, G., et al. (2012). TROPOMI on the ESA Sentinel-5 Precursor: A GMES mission for global observations of the atmospheric composition for climate, air quality and ozone layer applications. *Remote Sensing of Environment*, *120*, 70–83. https://doi.org/10.1016/j.rse.2011.09.027

Veres, P. R., Neuman, J. A., & Ryerson, T. B. (2019). ATom: L2 measurements from the NOAA ToF Chemical Ionization Mass Spectrometer (CIMS) [Dataset]. ORNL Distributed Active Archive Center. https://doi.org/10.3334/ORNLDAAC/1745

Verhoelst, T., Compernolle, S., Pinardi, G., Lambert, J.-C., Eskes, H. J., Eichmann, K.-U., et al. (2021). Ground-based validation of the Copernicus Sentinel-5p TROPOMI NO_2 measurements with the NDACC ZSL-DOAS, MAX-DOAS and Pandonia global networks. *Atmospheric Measurement Techniques*, *14*(1), 481–510. https://doi.org/10.5194/amt-14-481-2021

Viscardy, S., Errera, Q., Christophe, Y., Chabrillat, S., & Lambert, J.-C. (2010). Evaluation of ozone analysis from UARS MLS assimilation by BASCOE between 1992 and 1997. *IEEE Journal of Selected Topics in Applied Earth Observations and Remote Sensing*, *3*(2), 190–202. https://doi.org/10.1109/JSTARS.2010.2040463

Vogt, R., Crutzen, P. J., & Sander, R. (1996). A mechanism for halogen release from sea-salt aerosol in the remote marine boundary layer. *Nature*, *383*(6598), 327–330. https://doi.org/10.1038/383327a0

Volkamer, R., Baidar, S., Campos, T. L., Coburn, S., DiGangi, J. P., Dix, B., et al. (2015). Aircraft measurements of BrO, IO, glyoxal, NO_2, H_2O, O_2–O_2 and aerosol extinction profiles in the tropics: Comparison with aircraft-/ship-based in situ and lidar measurements. *Atmospheric Measurement Techniques*, *8*(5), 2121–2148. https://doi.org/10.5194/amt-8-2121-2015

von Glasow, R. (2010). Atmospheric chemistry in volcanic plumes. *Proceedings of the National Academy of Sciences*, *107*(15), 6594–6599. https://doi.org/10.1073/pnas.0913164107

von Glasow, R., Bobrowski, N., & Kern, C. (2009). The effects of volcanic eruptions on atmospheric chemistry. *Chemical Geology*, *263*(1–4), 131–142. https://doi.org/10.1016/j.chemgeo.2008.08.020

von Glasow, R., Sander, R., Bott, A., & Crutzen, P. J. (2002a). Modeling halogen chemistry in the marine boundary layer. 1. Cloud-free MBL. *Journal of Geophysical Research*, *107D*, 4341. https://doi.org/10.1029/2001JD000942

von Glasow, R., Sander, R., Bott, A., & Crutzen, P. J. (2002b). Modeling halogen chemistry in the marine boundary layer. 2. Interactions with sulfur and the cloud-covered MBL. *Journal of Geophysical Research*, *107D*, 4323. https://doi.org/10.1029/2001JD000943

von Glasow, R., von Kuhlmann, R., Lawrence, M., Platt, U., & Crutzen, P. (2004). Impact of reactive bromine chemistry in the troposphere. *Atmospheric Chemistry and Physics*, *4*(11/12), 2481–2497. https://doi.org/10.5194/acp-4-2481-2004

Wang, S., Schmidt, J. A., Baidar, S., Coburn, S., Dix, B., Koenig, T. K., et al. (2015). Active and widespread halogen chemistry in the tropical and subtropical free troposphere. *Proceedings of the National Academy of Sciences*, *112*(30), 9281–9286. https://doi.org/10.1073/pnas.1505142112

Wang, X., Jacob, D. J., Downs, W., Zhai, S., Zhu, L., Shah, V., et al. (2021). Global tropospheric halogen (Cl, Br, I) chemistry and its impact on oxidants. *Atmospheric Chemistry and Physics*, *21*(18), 13973–13996. https://doi.org/10.5194/acp-21-13973-2021

Wang, X., Jacob, D. J., Eastham, S. D., Sulprizio, M. P., Zhu, L., Chen, Q., et al. (2019). The role of chlorine in global tropospheric chemistry. *Atmospheric Chemistry and Physics*, *19*(6), 3981–4003. https://doi.org/10.5194/acp-19-3981-2019

Wennberg, P. (1999). Bromine explosion. *Nature*, *397*(6717), 299–301. https://doi.org/10.1038/16805

Wennberg, P., Cohen, R., Stimpfle, R., Koplow, J., Anderson, J., Salawitch, R., et al. (1994). Removal of stratospheric O_3 by radicals: In situ measurements of OH, HO_2, NO, NO_2, ClO, and BrO. *Science*, *266*(5184), 398–404. https://doi.org/10.1126/science.266.5184.398

Wofsy, S. C., & ATom Science Team. (2018). ATom: Aircraft flight track and navigational data [Dataset]. ORNL Distributed Active Archive Center. https://doi.org/10.3334/ORNLDAAC/1613

Womack, C. C., Chace, W. S., Wang, S., Baasandorj, M., Fibiger, D. L., Franchin, A., et al. (2023). Midlatitude ozone depletion and air quality impacts from industrial halogen emissions in the Great Salt Lake Basin. *Environmental Science & Technology*, *57*(5), 1870–1881. https://doi.org/10.1021/acs.est.2c05376

Xia, M., Wang, T., Wang, Z., Chen, Y., Peng, X., Huo, Y., et al. (2022). Pollution-derived Br_2 boosts oxidation power of the coastal atmosphere. *Environmental Science & Technology*, *56*(17), 12055–12065. https://doi.org/10.1021/acs.est.2c02434

Yang, X., Blechschmidt, A.-M., Bognar, K., McClure-Begley, A., Morris, S., Petropavlovskikh, I., et al. (2020). Pan-Arctic surface ozone: Modelling vs. measurements. *Atmospheric Chemistry and Physics*, *20*(24), 15937–15967. https://doi.org/10.5194/acp-20-15937-2020

Yang, X., Cox, R. A., Warwick, N. J., Pyle, J. A., Carver, G. D., O'Connor, F. M., & Savage, N. H. (2005). Tropospheric bromine chemistry and its impacts on ozone: A model study. *Journal of Geophysical Research*, *110*(D23), D23311. https://doi.org/10.1029/2005JD006244

Yang, X., Frey, M. M., Rhodes, R. H., Norris, S. J., Brooks, I. M., Anderson, P. S., et al. (2019). Sea salt aerosol production via sublimating wind-blown saline snow particles over sea ice: Parameterizations and relevant microphysical mechanisms. *Atmospheric Chemistry and Physics*, *19*(13), 8407–8424. https://doi.org/10.5194/acp-19-8407-2019

Yang, X., Pyle, J. A., & Cox, R. A. (2008). Sea salt aerosol production and bromine release: Role of snow on sea ice. *Geophysical Research Letters*, *35*(16), L16815. https://doi.org/10.1029/2008GL034536

Yang, X., Pyle, J. A., Cox, R. A., Theys, N., & Van Roozendael, M. (2010). Snow-sourced bromine and its implications for polar tropospheric ozone. *Atmospheric Chemistry and Physics*, *10*(16), 7763–7773. https://doi.org/10.5194/acp-10-7763-2010

Zhao, X., Strong, K., Adams, C., Schofield, R., Yang, X., Richter, A., et al. (2016). A case study of a transported bromine explosion event in the Canadian high Arctic. *Journal of Geophysical Research: Atmospheres*, *121*(1), 457–477. https://doi.org/10.1002/2015JD023711

Zhu, L., Jacob, D. J., Eastham, S. D., Sulprizio, M. P., Wang, X., Sherwen, T., et al. (2019). Effect of sea salt aerosol on tropospheric bromine chemistry. *Atmospheric Chemistry and Physics*, *19*(9), 6497–6507. https://doi.org/10.5194/acp-19-6497-2019

Zhu, L., Jacob, D. J., Mickley, L. J., Marais, E. A., Cohan, D. S., Yoshida, Y., et al. (2014). Anthropogenic emissions of highly reactive volatile organic compounds in eastern Texas inferred from oversampling of satellite (OMI) measurements of HCHO columns. *Environmental Research Letters*, *9*(11), 114004. https://doi.org/10.1088/1748-9326/9/11/114004

Zhu, L., Mickley, L. J., Jacob, D. J., Marais, E. A., Sheng, J., Hu, L., et al. (2017). Long-term (2005–2014) trends in formaldehyde (HCHO) columns across North America as seen by the OMI satellite instrument: Evidence of changing emissions of volatile organic compounds. *Geophysical Research Letters*, *44*(13), 7079–7086. https://doi.org/10.1002/2017GL073859